JEM Journal of Experimental Medicine

ARTICLE

Thymic epithelial cells require lipid kinase Vps34 for CD4 but not CD8 T cell selection

J. Luke Postoak[1], Wenqiang Song[1], Guan Yang[1], Xingyi Guo[2], Shiyun Xiao[3], Cherie E. Saffold[1], Jianhua Zhang[4,5], Sebastian Joyce[1,6], Nancy R. Manley[3], Lan Wu[1], and Luc Van Kaer[1]

The generation of a functional, self-tolerant T cell receptor (TCR) repertoire depends on interactions between developing thymocytes and antigen-presenting thymic epithelial cells (TECs). Cortical TECs (cTECs) rely on unique antigen-processing machinery to generate self-peptides specialized for T cell positive selection. In our current study, we focus on the lipid kinase Vps34, which has been implicated in autophagy and endocytic vesicle trafficking. We show that loss of Vps34 in TECs causes profound defects in the positive selection of the CD4 T cell lineage but not the CD8 T cell lineage. Utilizing TCR sequencing, we show that T cell selection in conditional mutants causes altered repertoire properties including reduced clonal sharing. cTECs from mutant mice display an increased abundance of invariant chain intermediates bound to surface MHC class II molecules, indicating altered antigen processing. Collectively, these studies identify lipid kinase Vps34 as an important contributor to the repertoire of selecting ligands processed and presented by TECs to developing CD4 T cells.

Introduction

The thymus is a specialized primary lymphoid organ that functions to generate a pool of immunologically competent T cells that can recognize and eliminate foreign antigens while tolerating the body's own tissues (Kadouri et al., 2020). T cells sense cognate peptide antigens bound to MHC molecules through their diverse TCRs that are highly specific for a particular peptide–MHC complex. The generation of a broad and tolerant TCR repertoire is mainly directed by self-peptide/MHC complexes displayed by thymic epithelial cells (TECs) during thymocyte development in a process called thymic selection (Han and Zuniga-Pflucker, 2021; Takaba and Takayanagi, 2017). Cortical TECs (cTECs) present self-peptides bound to MHC class I or class II molecules to immature $CD4^+CD8^+$ (double-positive [DP]) thymocytes for positive selection of $CD8^+$ or $CD4^+$ (single-positive [SP]) T cells, respectively. Here, TCR engagement with low avidity or antagonistic peptide–MHC complexes provides prosurvival signals (Klein et al., 2014).

MHC class II–mediated antigen presentation in cTECs relies on cellular processes and machinery that are unique among APCs (Kondo et al., 2017). While most APCs depend on extracellular sources to supply peptides for MHC class II binding, cTECs predominantly rely on intracellular sources for this process (Klein et al., 2014). In addition to utilizing a unique spectrum of endosomal and lysosomal proteases and relying on distinct machinery for trafficking of membrane proteins, a high frequency of cTECs is constitutively active in macroautophagy (Mizushima et al., 2004; Nedjic et al., 2008; Schuster et al., 2015). Macroautophagy (hereafter called autophagy) is a catabolic cellular process that targets components of the cytosol to the lysosome for degradation and recycling (Levine and Kroemer, 2019). A previous study provided evidence that autophagosomal vesicles constantly fuse with the MHC class II peptide-loading compartment to facilitate antigen presentation (Schmid et al., 2007), raising the possibility that the autophagy pathway contributes to the repertoire of self-peptides that binds MHC class II molecules and is optimized for positive selection of $CD4^+$ T cells. Autophagy has common features with endocytosis and vesicle trafficking with which it shares effector molecules, including several of the autophagy-related (Atg) factors (Galluzzi and Green, 2019). However, how these processes and their shared machinery regulate antigen presentation remains incompletely understood.

[1]Department of Pathology, Microbiology and Immunology, Vanderbilt University School of Medicine, Nashville, TN; [2]Department of Biomedical Informatics, Vanderbilt University School of Medicine, Nashville, TN; [3]Department of Genetics, University of Georgia, Athens, GA; [4]Department of Pathology, University of Alabama at Birmingham, Birmingham, AL; [5]Birmingham Veterans Affairs Medical Center, Birmingham, AL; [6]Department of Veterans Affairs, Tennessee Valley Healthcare System, Nashville, TN.

Correspondence to Luc Van Kaer: luc.van.kaer@vumc.org

Guan Yang's present address is Department of Infectious Diseases and Public Health, City University of Hong Kong, Kowloon Tong, Hong Kong.

Vacuolar protein sorting 34 (Vps34, also called Pik3c3 [phosphatidylinositol 3-kinase catalytic subunit type 3]) is a class III phosphoinositide 3-kinase (PI3K) that plays a role in endocytosis, intracellular vesicular trafficking, and autophagosome formation during autophagy (Backer, 2016). Vps34-deficient dendritic cells display defective autophagic flux leading to the accumulation of aggregated cellular proteins and organelles (Parekh et al., 2017). Loss of Vps34 also significantly attenuated the CD4$^+$ T cell stimulatory capacity of dendritic cells in response to a central nervous system–derived autoantigen that relies on the extracellular route of antigen processing (Yang et al., 2022). However, whether Vps34-mediated cellular processes regulate the intracellular route for MHC class II–mediated antigen processing that TECs rely on to generate a broad CD4$^+$ TCR repertoire is unknown.

In the present study, we generated mice with a TEC-specific deletion of *Vps34* to determine its effects on the antigen-presenting function of TECs. Our findings revealed a critical role for Vps34 in the capacity of TECs to facilitate the positive selection of CD4$^+$ but not CD8$^+$ T cells in a manner independent of the canonical, Atg5-dependent autophagy pathway.

Results

TEC-specific Vps34 deficiency causes progressive thymic hypoplasia, blunted thymopoiesis, and T cell lymphopenia

To determine the function of Vps34 in TECs, we used mice expressing Cre recombinase from the endogenous *Foxn1* locus, with high Cre activity within TECs and their precursors (Gordon et al., 2007). To confirm Cre activity, we crossed Foxn1-Cre transgenic mice to Ai14 mice, which contain a floxed-stop-tdTomato reporter cassette knocked into the *Rosa26* locus (Madisen et al., 2010). Flow cytometric analysis confirmed Cre reporter activity in TECs of Cre$^+$ Ai14$^+$ mice but not Cre$^-$ controls or in CD45$^+$ cells from either group (Fig. S1 A). Next, we crossed Foxn1-Cre mice with mice carrying a floxed allele of the *Vps34* gene (Jaber et al., 2012) to generate mice with a TEC-specific loss of Vps34 (hereafter referred to as Vps34^{TEC} mice). These animals were born at the expected Mendelian ratios and, apart from altered thymic development described below, did not show any obvious anatomic abnormalities, including the skin where Foxn1 is expressed by keratinocytes (Fig. S1 B; Gordon et al., 2007). Gross examination of the thoracic cavity revealed similar thymic size at 1 wk of age but severely hypoplastic thymi by 4 wk of age in Vps34^{TEC} mice (Figs. 1 A and S1 C). Coincident with thymic atrophy, Vps34^{TEC} mice displayed a progressive loss in thymic cellularity (Fig. 1 B). Additionally, Vps34^{TEC} mice had a progressive loss in CD4$^+$CD8$^+$ DP thymocytes, indicating a severe loss in thymic function by 3 wk of age (Fig. 1 C). Analysis of the development of CD4$^-$CD8$^-$ double-negative (DN) thymocytes in young adult animals revealed accumulation of thymocytes at the CD44$^+$CD25$^-$ DN1 and CD44$^-$CD25$^-$ DN4 stages (Fig. S1 D), further highlighting the extent of thymic dysfunction in mutant animals. This loss of thymic function was associated with significant T cell lymphopenia in adult Vps34^{TEC} mice, with a relatively stronger effect on the CD4$^+$ than the CD8$^+$ T cell compartment (Fig. 1 D). Consistent with the observed T cell lymphopenia, mature T cells in the periphery of Vps34^{TEC} mice displayed a more activated phenotype as revealed by a decrease in the frequency of naive CD44^{lo}CD62L^{hi} T cells (Fig. 1 E), likely resulting from increased homeostatic proliferation. These data indicate that Vps34^{TEC} mice exhibit rapid thymic involution, with profound loss of thymic function as the animals become juveniles, an age when thymic function normally peaks (Baran-Gale et al., 2020; Manley et al., 2011).

Vps34 deficiency disrupts autophagy and alters cellularity and morphology in TECs

Autophagy in mouse TECs occurs constitutively at levels detectable by reporter alleles, making it unique among mammalian tissue, where most other cell types require inducing stimuli such as starvation to measure autophagic flux (Mizushima et al., 2004). Many studies have identified a critical requirement for Vps34 expression in multiple mammalian tissues for the constitutive or induced generation of autophagy (Jaber et al., 2012; Parekh et al., 2017; Parekh et al., 2013; Zhou et al., 2010). Nevertheless, situations where autophagy can be induced in a Vps34-independent manner have also been described (Boukhalfa et al., 2020; Martinez-Martin et al., 2017). To measure the contribution of Vps34 to autophagy in TECs, we used an autophagy reporter strain that expresses transgenic LC3 (microtubule-associated protein 1A/1B-light chain 3) that is dually labeled with EGFP and RFP (Li et al., 2014). During autophagy, cytosolic LC3 is recruited to the autophagosome, where it is labeled with both EGFP and RFP. As an autophagosome matures, it fuses with the lysosome and acidifies, which quenches the pH-sensitive EGFP (Fig. 2 A). Flow cytometric analysis of TECs isolated from reporter$^+$ WT controls showed an RFP$^+$EGFP$^+$ DP population indicating cytosolic and autophagosomal LC3 and an RFP$^+$EGFP^{lo} population representing autolysosomes (Fig. 2 B). This confirms previous reports that autophagy is active in TECs under physiological conditions (Mizushima et al., 2004; Nedjic et al., 2008; Schuster et al., 2015). In TECs isolated from reporter$^+$ Vps34^{TEC} mice, we found a significant decrease in the frequency of EGFP^{lo} cells among the RFP$^+$ population, indicating a block in autophagic flux and confirming an essential role for Vps34 in TEC autophagy.

To assess the effects of Vps34 loss on TEC cellularity and morphology, we focused our analysis on the neonatal age before extensive atrophy occurs in Vps34^{TEC} mice. Histological examination of thymic morphology revealed a disruption of thymic architecture in Vps34^{TEC} mice. H&E staining and immunofluorescence analysis with the medullary TEC (mTEC)–specific markers Keratin-5 and UEA-1 showed disruption of the medulla and cortex organization in Vps34^{TEC} mice resulting in smaller and more diffuse medullary islets at 3 d of age that became more profound by 10 d of age (Figs. 2 C and S1 E). To quantify these effects of Vps34 deficiency, we analyzed TECs by flow cytometry, which revealed a significant decrease in the frequency and number of EpCAM$^+$CD45$^-$ TECs at postnatal days 3 and 10 (Figs. 2 D and S1 F). Among TEC subsets, there was a relative loss in the frequency of mTECs (Ly-51$^-$UEA-1$^+$) compared with cTECs (Ly-51$^+$UEA-1$^-$) in Vps34^{TEC} mice vs. control mice (Figs. 2 E and S1 G), which agreed with the histological analysis. Interestingly,

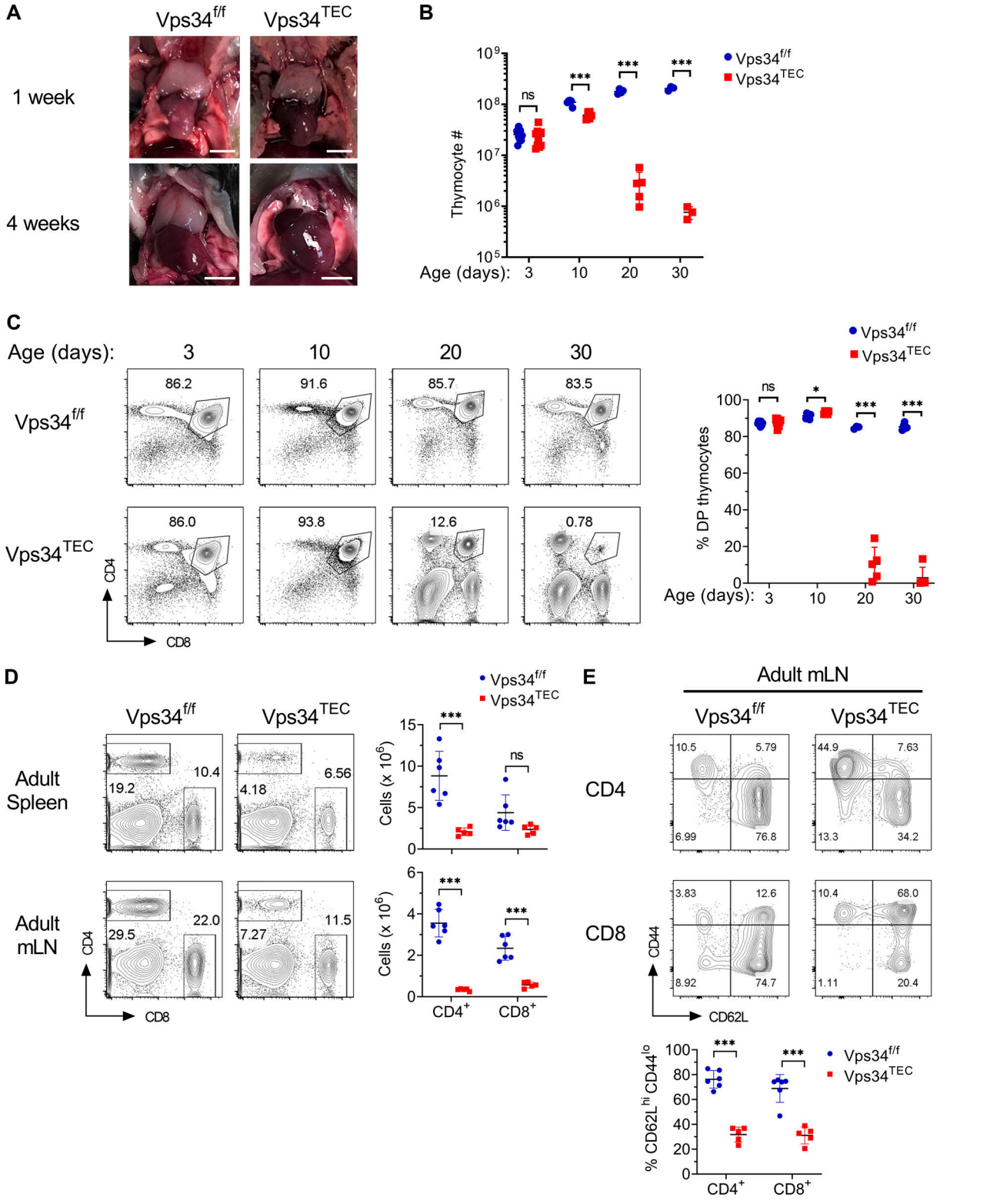

Figure 1. **Vps34 deficiency in TECs causes thymic hypoplasia, decreased thymopoiesis, and T cell lymphopenia. (A)** Thoracic cavity at 1 wk (top, scale bar = 0.5 cm) and 4 wk (bottom, scale bar = 0.4 cm) of age in Vps34$^{f/f}$ or Vps34^{TEC} mice. **(B)** Total thymocyte cellularity at the indicated ages in Vps34$^{f/f}$ or Vps34^{TEC} mice. **(C)** Flow cytometric analysis of CD4 and CD8 DP thymocytes at the indicated ages in Vps34$^{f/f}$ or Vps34^{TEC} mice. The graph represents the frequency of DP thymocytes among all thymocytes. Data for A–C obtained from two or three independent experiments (n = 3–10 mice per genotype). **(D)** CD4 and CD8 expression profiles of T cells isolated from spleen (top) and mesenteric lymph nodes (mLN; bottom) in 7-wk-old Vps34$^{f/f}$ or Vps34^{TEC} mice. Graphs represent total CD4$^+$ T cells (CD4$^+$CD3$^+$) and CD8$^+$ T cells (CD8$^+$CD3$^+$) in the spleen (top) and mLN (bottom). **(E)** CD44 and CD62L expression profiles of T cells isolated from the mLN of 7-wk-old Vps34$^{f/f}$ or Vps34^{TEC} mice. Graphs represent the frequency of CD62L^{hi}CD44^{lo} cells among total CD4$^+$ T cells (top panels) or total CD8$^+$ T cells (bottom panels). Data for D and E obtained from two independent experiments (n = 5–6 mice per genotype). Data signify the mean ± SD where each data point represents a biological replicate. *, P < 0.05; ***, P < 0.001; ns, not significant by unpaired t test.

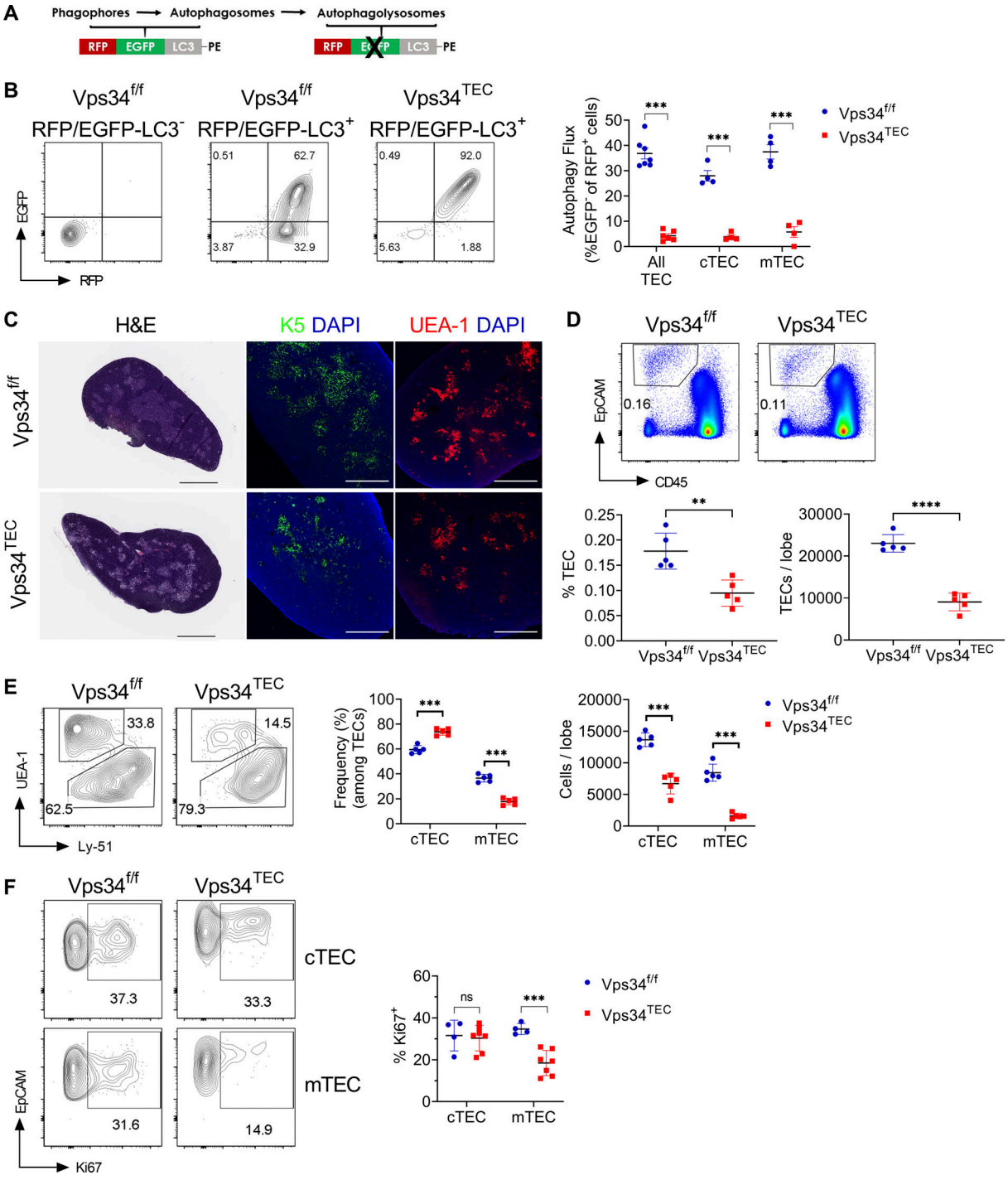

Figure 2. **TEC-specific Vps34 deficiency modulates TEC autophagy, cellularity, and morphology. (A)** Schematic of LC3-EGFP/RFP reporter. **(B)** Flow cytometric analysis of TECs (CD45⁻EpCAM⁺) for LC3-EGFP/RFP reporter expression in nontransgenic control (left), Vps34$^{f/f}$ (middle), and Vps34^{TEC} (right) mice at 3 d of age. The graph represents percent EGFP^{lo} TECs, cTECs (UEA-1⁻ TECs), and mTECs (UEA-1⁺ TECs) among corresponding RFP⁺ TEC populations. Data are representative of four (for all TECs) and two (for cTEC and mTEC) independent experiments. **(C)** Thymus tissue sections from 3-d-old Vps34$^{f/f}$ or Vps34^{TEC} mice were stained with H&E (scale bar = 800 µm), anti-keratin 5 (K5; green) and DAPI (blue), or UEA-1 lectin (red) and DAPI (blue; scale bar = 500 µm). Data are representative of three independent experiments with three biological replicates. **(D and E)** Flow cytometric analysis of total TECs (D) and TEC subsets (E), including mTECs (UEA-1⁺Ly-51⁻) and cTECs (UEA-1⁻Ly-51⁺) at 3 d of age. Graphs represent frequency (left) and total number (right) of TECs or TEC subsets. **(F)** Ki67 expression among cTECs (MHC II^{hi}UEA-1⁻ TECs) and mTECs (MHC II^{hi}UEA-1⁺ TECs). The graph represents frequency of Ki67⁺ cells among TEC subsets. Data for D–F obtained from two independent experiments with four to seven biological replicates. Data signify the mean ± SD where each data point represents a biological replicate in all graphs. **, P < 0.01; ***, P < 0.001; ns, not significant by unpaired *t* test. PE, phosphatidylethanolamine.

mTECs isolated from mutant mice also displayed a more immature (mTEC^{lo}) phenotype as gleaned from lower surface expression of the antigen presentation-associated molecules MHC class II and CD80 (Fig. S1 H). We next considered that alterations in cellular proliferation may contribute to decreases in TEC cellularity in Vps34^{TEC} mice. We performed flow cytometric analyses for intracellular Ki67 expression in TEC populations isolated from Vps34^{TEC} neonatal mice. Compared with littermate controls, we found significant decreases in cell cycling in Vps34-deficient mTECs but not cTECs (Fig. 2 F). This suggests that the defects seen in mTEC cellularity in Vps34^{TEC} mice can be partially explained by a loss of proliferating mTECs. These data indicate that TECs require Vps34 for normal cellularity in neonatal mice and that loss of Vps34 results in a progressive loss of TEC cellularity, with more profound effects on mTECs than cTECs.

Postnatal deletion of Vps34 decreases TEC cellularity and homeostasis

Because the hypoplastic thymi observed in Vps34^{TEC} mice could be caused by a loss of TEC progenitors (TEPC) during development, it is unclear if TECs require Vps34 expression to maintain their homeostasis in adulthood. To address this question, we analyzed neonatal mice for putative TEPC populations (Wong et al., 2014) to test if there are defects in the establishment of postnatal TEPCs in Vps34^{TEC} mice. We identified the putative TEPC population as CD45^{-}EpCAM^{+}UEA-1^{lo}Itga6^{+}Sca-1^{+} cells. Our analysis revealed no significant difference in the numbers of putative TEPCs in postnatal day 3 Vps34^{TEC} mice compared with littermate controls (Fig. S1 I). To further test whether there is an ongoing requirement for Vps34 function in TEC homeostasis, we used an inducible deletion system in which ablation of Vps34 can be achieved specifically in the thymic stroma after the microenvironment has been fully established. Thymic lobes from newborn Rosa26-CreER^{T2};Vps34$^{f/f}$ or Vps34$^{f/f}$ mice were grafted under the kidney capsule of adult C57BL/6 mice. Host hematopoietic cells were allowed to reconstitute for 3 wk, and Cre-ER^{T2}–mediated deletion of *Vps34* was induced by tamoxifen administration, whereas control Rosa26-CreER^{T2};Vps34$^{f/f}$ mice were treated with vehicle, and a second control group of Vps34$^{f/f}$ mice were also treated with tamoxifen. Host kidney capsules were collected 3 wk after administration of the last tamoxifen or vehicle dose, and the grafted thymic lobes were analyzed (Fig. 3 A). The size and cellularity of grafts isolated from tamoxifen-treated Rosa26-CreER^{T2};Vps34$^{f/f}$ mice were significantly reduced compared with both groups of control mice (Fig. 3 B). Additionally, flow cytometric analysis revealed that TEC numbers were also significantly reduced in the Vps34-deficient grafts compared with the controls (Fig. 3 C). These results indicate a postnatal requirement of Vps34 in TECs to maintain thymopoiesis and TEC homeostasis.

Altered T cell development in neonatal Vps34^{TEC} mice

Given the essential role Vps34 plays in endocytosis, vesicle trafficking, and autophagy (Bilanges et al., 2019), cellular processes that can influence antigen presentation (Roche and Furuta, 2015), we next investigated intrathymic development of T cells in neonatal Vps34^{TEC} mice. Because DN thymocyte development is significantly disrupted in adult Vps34^{TEC} mice, we analyzed DN thymocyte subsets in neonatal mice. We did not observe alterations in the frequency or cellularity of DN subsets, including early thymic progenitors (ETPs; Fig. S2 A). This finding indicates that TECs do not require Vps34 for DN thymocyte development in neonates, a time period before extensive loss of thymic cellularity. However, we observed similar frequency and numbers of DP thymocytes in mutant mice compared with controls, but a relative decrease in CD4 SP and a relative increase in CD8 SP cells (Fig. 4 A). Similar shifts in the distribution of T cell subsets were observed in the spleen of mutant mice (Fig. S2 B). To further investigate thymic selection, we analyzed CD4 and CD8 expression on developing thymocytes at discrete developmental stages. Developing thymocytes undergo sequential stages of TCRβ and CD69 cell surface expression that provide phenotypic markers of T cell positive selection (Barthlott et al., 1997). Under physiological conditions, positive selection sets off a transient upregulation of CD69 among TCRβ^{int} thymocytes (stage II). In turn, these cells sequentially adopt a TCRβ^{hi}CD69^{+} (stage III) and eventually a TCRβ^{hi}CD69^{lo} (stage IV) cell surface phenotype as they move from the DP toward the CD4 SP or CD8 SP lineages. The relative frequencies of these distinct thymocyte populations were undisturbed in neonatal Vps34^{TEC} mice (Fig. 4 B). However, at stages III and IV, there was an increase in the frequency of thymocytes that retained CD4 and CD8 DP expression. Further, the thymocytes at stages III and IV were more skewed toward the CD8 SP lineage in Vps34^{TEC} mice (Fig. 4 B).

Given the alterations in SP thymocytes, we also analyzed maturation in SP subsets. Following positive selection, SP thymocytes express high surface levels of CD24 (heat-stable antigen), which they downregulate as they mature (Nikolic-Zugic and Bevan, 1990; Ramsdell et al., 1991). Interestingly, we observed no alterations in the frequency of mature TCRβ^{hi}CD24^{lo} cells among CD4 SP thymocytes but an increase in the frequency of these cells among CD8 SP thymocytes (Fig. 4 C). This finding implies that the alterations seen in CD4 SP selection in Vps34^{TEC} mice are unlikely to be due to defects in postselection maturation.

An important subset of CD4 SP thymocytes is thymic regulatory T cells (tTregs), which are essential for maintaining immune tolerance and can be identified by the lineage-defining transcription factor Foxp3 (Savage et al., 2020). mTECs are critical for the development of tTregs (Cowan et al., 2013). Given the observed defects in the mTEC compartment of Vps34^{TEC} mice, we next analyzed tTreg development, using a Foxp3-RFP knock-in reporter line crossed onto Vps34^{TEC} mice. We observed no alterations in the frequency of Foxp3^{+}CD25^{+} Tregs among CD4 SP thymocytes (Fig. 4 D) or CD4^{+} splenocytes (Fig. S2 C). These observations indicate that Vps34 in TECs is dispensable for the thymic development of Tregs.

Finally, we assessed the thymic development of two nonconventional T cell subsets, invariant natural killer T (iNKT) and mucosal associated invariant T (MAIT) cells, that are positively selected on DP thymocytes (Mayassi et al.,

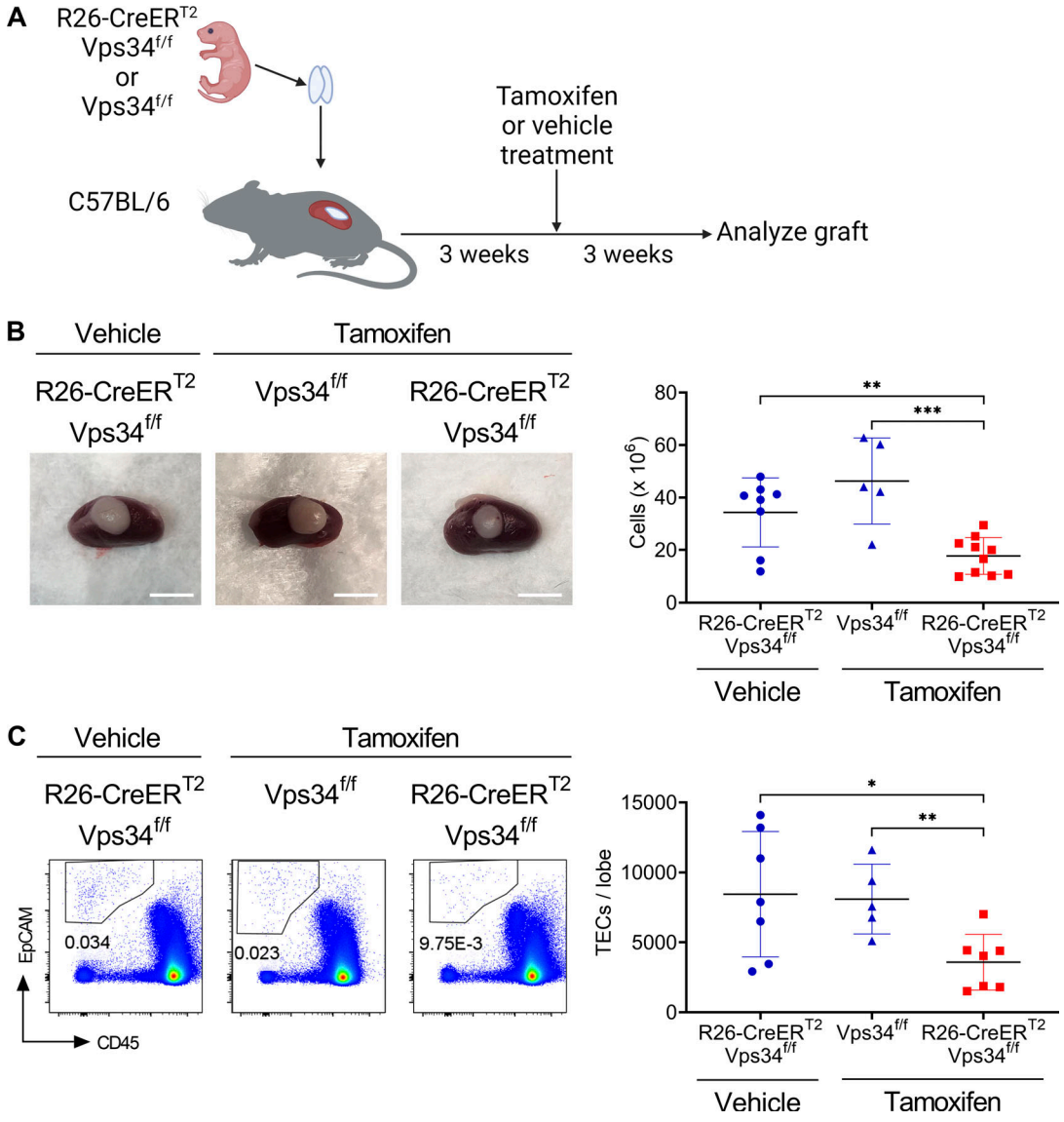

Figure 3. **Postnatal deletion of Vps34 in thymic stromal cells decreases cellularity and TEC homeostasis in a transplant model. (A)** Schematic of the experimental design. Thymic lobes isolated from newborn Rosa26-CreER^{T2}; Vps34$^{f/f}$, or Vps34$^{f/f}$ mice were transplanted under the kidney capsule of 6–8-wk-old C57BL/6 recipient mice. Recipients were treated with tamoxifen or vehicle by oral gavage 3 wk after grafting and were analyzed 3 wk after the last tamoxifen treatment. **(B)** Examples of kidneys transplanted with a thymus lobe from vehicle- or tamoxifen-treated recipient mice (scale bar = 0.5 cm). The graph represents total cellularity from transplanted thymi. **(C)** Flow cytometric analysis of TECs isolated from vehicle- or tamoxifen-treated mice. The graph represents total TEC cellularity (CD45$^-$EpCAM$^+$ cells) from transplanted thymi. Data signify the mean ± SD. Data are representative of four independent experiments where each data point represents a biological replicate. *, P < 0.05; **, P < 0.01; ***, P < 0.001 by unpaired *t* test.

2021). Prior studies have shown that iNKT cell development is impacted by mTECs (Lucas et al., 2020). We used PBS57/CD1d-tetramers to identify iNKT cells, which were present among thymocytes from adult Vps34$^{f/f}$ but not CD1d knock-out mice (Fig. S2 D). Consistent with a previous report (Benlagha et al., 2005), we found iNKT cells to be very rare in the thymus of neonatal mice, and we were unable to detect significant differences between Vps34$^{fl/fl}$ and Vps34^{TEC} mice (Fig. S2 D). We next used 5-OP-RU/MR1 tetramers to identify MAIT cells and 6-FP/MR1 tetramers for control staining. Similar to iNKT cells, we found MAIT cells to be very rare in the thymus of both neonatal control and Vps34^{TEC} mice (Fig. S2 E).

Vps34 regulates positive selection of MHC class II–restricted transgenic TCRs

To further investigate the contribution of TEC-specific Vps34 to T cell positive selection, we tested the development and selection of T cells expressing antigen-specific, MHC class I– or class II–restricted TCRs in transgenic animals. Although such studies are often performed with TCR transgenic bone marrow chimeras, we opted against this approach owing to the severe thymic hypoplasia in Vps34^{TEC} mice. Instead, we bred individual TCR transgenic lines with the Vps34^{TEC} mice and compared these animals with their Cre$^-$ littermate controls at 7–10 d of age. We did not observe any defects in the frequency or numbers of CD8 SP thymocytes for the MHC class I–restricted OTI or P14 lines

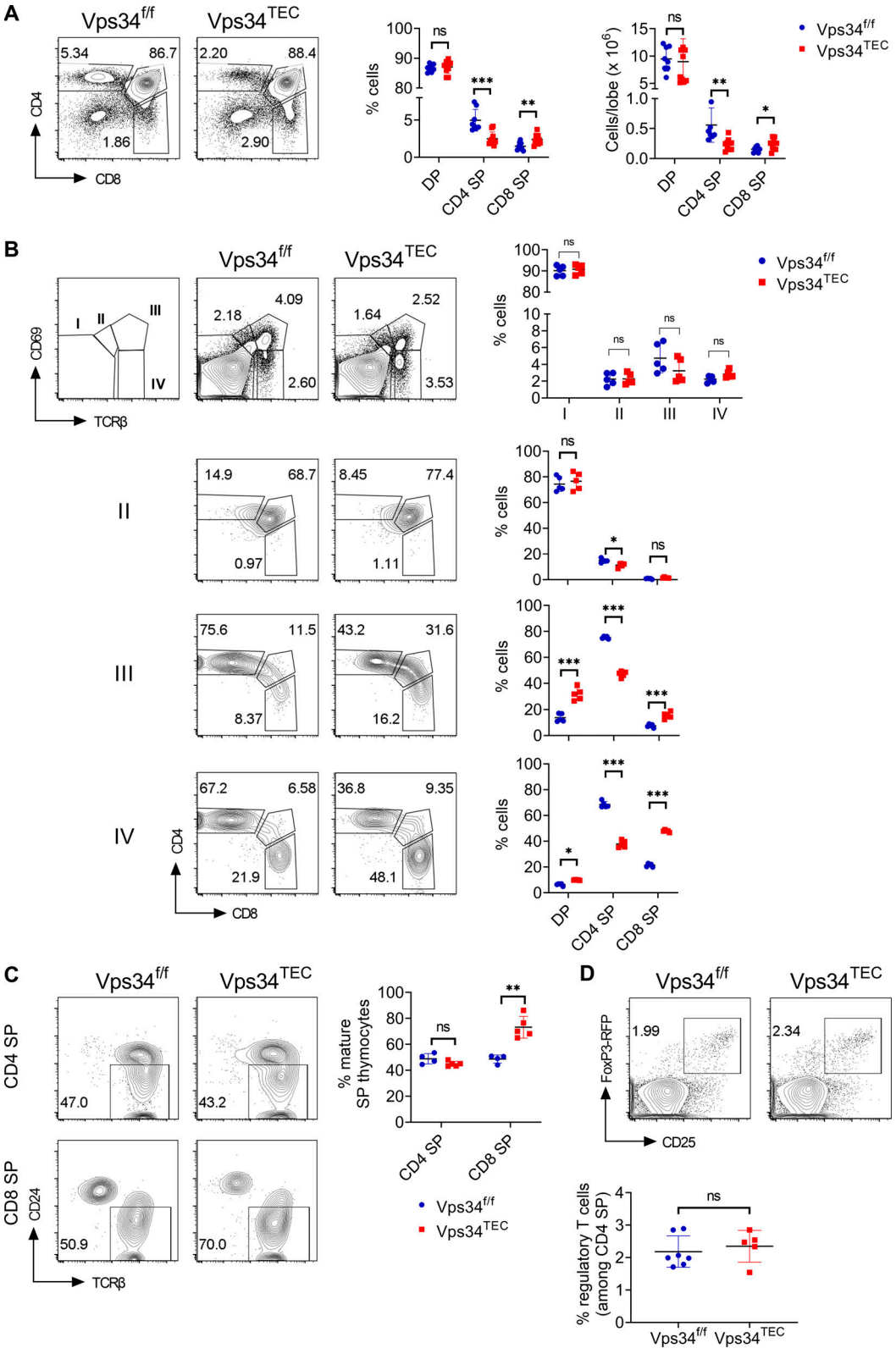

Figure 4. **Defective CD4⁺ T cell development in neonatal Vps34^{TEC} mice.** Thymocytes from 3-d-old Vps34$^{f/f}$ or Vps34^{TEC} mice were analyzed by flow cytometry. **(A)** CD4 and CD8 expression. Graphs represent frequency and total numbers of indicated thymocyte subsets. Data obtained from three independent experiments (n = 8–10 mice per genotype). **(B and C)** CD69 and TCRβ expression (top panel) on thymocytes was used to gate on the indicated developmental thymocyte stages, and the percentage of cells within each stage is depicted in the graph at the top. Cells within stages II–IV were then analyzed for CD4 and CD8 surface expression. Graphs represent the frequency of DP, CD4 SP, and CD8 SP thymocytes within each specified developmental stage (B) and CD24 and TCRβ expression (C). The graph represents the frequency of mature thymocytes (TCRβ⁺CD24^{lo}) among the CD4 SP or CD8 SP subsets. Data for B

and C obtained from two independent experiments (n = 4–5 mice per genotype). **(D)** Foxp3-RFP and CD25 expression of cells within the CD4 SP CD3$^+$ gate. The graph represents the frequency of thymic regulatory T cells (Foxp3-RFP$^+$CD25$^+$) among CD4 SP CD3$^+$ thymocytes. Data obtained from three independent experiments (n = 5–7 mice per genotype). Data signify the mean ± SD where each data point represents a biological replicate. *, P < 0.05; **, P < 0.01; ***, P < 0.001; ns, not significant by unpaired t test.

(see Table S1 for the specificities of the transgenic TCRs). We also did not find any alterations in the expression of the clonotypic TCRs of these lines among CD8 SP cells (Fig. 5, A–C). In contrast, a near-complete block in development from the DP to CD4 SP thymocyte stage occurred in each of the MHC class II–restricted TCR transgenic lines, OTII, LLO56, LLO118, and female Marilyn mice. Additionally, among the CD4 SP thymocytes, there was a decrease in the frequency of T cells expressing the clonotypic TCRs of individual transgenic lines (Fig. 5, D–H). Interestingly, the frequency of DP populations of some but not all transgenic TCRs was also altered (Fig. S3 A). These data indicate that Vps34 is required by TECs to positively select MHC class II–restricted but not MHC class I–restricted transgenic TCRs. Importantly, similar trends were observed in the spleen at 7–10 d of age. There was a slight decrease in the frequency of splenic OTI cells and total OTI and P14 splenocytes in the mutant mice (Fig. S3, B–D). This is likely due to decreased thymopoiesis independent of selection, because polyclonal Vps34^{TEC} mice analyzed at a similar age range exhibited a profound decrease in thymocyte cellularity (Fig. 1 B). However, there was an almost-complete absence of TCR transgenic CD4$^+$ splenocytes in Vps34^{TEC} mice (Fig. S3, E–I).

Appropriate TCR signal strength is crucial for thymic selection (Gascoigne et al., 2016). Surface CD5 expression on developing thymocytes positively correlates with TCR signal strength and can be used as a surrogate marker of TCR signal strength (Azzam et al., 1998). Interestingly, surface CD5 expression was decreased on DP thymocytes in transgenic lines expressing MHC class II–restricted but not class I–restricted TCRs (Fig. 5 I). This finding indicates that altered TCR signaling coincides with defective positive selection. It is possible that changes in self-peptide/MHC class II displayed on Vps34-deficient TECs leads to alterations in TCR signaling on developing MHC class II–restricted transgenic thymocytes and thus causes these defects in positive selection. Alternatively, given that Vps34^{TEC} mice display decreased cTEC cellularity, it is plausible that the reduced CD5 expression is due to developing thymocytes sensing fewer total numbers of self-peptide/MHC class II complexes. However, we disfavor this as an explanation considering that developing thymocytes similarly encounter fewer peptide/MHC class I complexes, yet CD5 signaling remains unaltered in MHC class I–restricted TCR transgenic Vps34^{TEC} mice (Fig. 5 I).

The Marilyn TCR transgenic system allows for the interrogation of negative selection in addition to positive selection (Lantz et al., 2000). Marilyn transgenic TCRs are specific for the male H-Y antigen. As such, developing Marilyn T cells undergo negative selection in the thymus of male but not female mice. We did not observe any differences in the thymic selection of Marilyn T cells in male Vps34^{TEC} mice compared with controls (Fig. S3 J). While this may suggest that negative selection (and thus the antigen processing and presentation of the male H-Y antigen) is intact in Vps34-deficient thymi, the severe defects in positive selection in female mice confound the interpretation of these observations.

Altered TCRβ chain gene usage and repertoire sharing in CD4 SP thymocytes of neonatal Vps34^{TEC} mice

To explore how Vps34-mediated cellular processes in TECs impact the CD4$^+$ TCR repertoire, we conducted deep sequencing of the complementarity-determining region 3 (CDR3) sequences of TCR Vβ chains of genomic DNA from CD4 SP TCRβ$^+$ thymocytes isolated from three neonatal Vps34^{TEC} mice and three littermate controls. TCR repertoire diversity was assessed using Simpson clonality index downsampled to 24,791 randomly chosen sequencing reads to correct for differences in the total productive templates sampled (Fig. 6 A). This analysis revealed that the repertoire diversity of CD4 SP T cells from Vps34^{TEC} mice was maintained similarly to control mice (Fig. 6 B). The hypervariable CDR3 of the TCR is crucial for antigen recognition, as it contacts MHC class II peptide complexes on APCs. The diversity in the CDR3 is generated through genetic recombination and by the addition of random nucleotides, producing CDR3s of variable length with a Gaussian-like distribution (Pannetier et al., 1993). Strikingly, we found that the CDR3 sequences in CD4 SP T cells from Vps34^{TEC} mice were longer compared with control mice (Fig. 6 C). We next assessed TCR Vβ region gene usage and noticed significant changes in the prevalence of 6 Vβ chain gene segments (Fig. 6 D). Importantly, the altered Vβ gene segments were not of low use frequency in controls. To further assess how Vps34 deficiency in TECs impacts the CD4$^+$ TCR Vβ repertoire, we calculated clonal overlap using the Morisita index (Fig. 6 E), which revealed significantly more clonal overlap among CD4 SP T cells from control animals than in any control-mutant repertoire comparisons. Intriguingly, there was also significantly lower clonal overlap among the repertoires of mutant animals compared with controls. Thus, while Vps34 in TECs is dispensable for maintaining CD4$^+$ TCR repertoire diversity, its absence leads to altered CDR3 length, Vβ gene usage, and repertoire sharing.

To explore functional consequences of the altered CD4$^+$ T cell development and repertoire in Vps34^{TEC} mice, we tested the response of these animals and littermate controls to experimental autoimmune encephalomyelitis (EAE), an animal model of human multiple sclerosis. Results showed a delayed onset of clinical disease in Vps34^{TEC} mice compared with littermate controls (Fig. S4 A). Mutant mice also experienced significantly reduced incidence and severity of disease (Fig. S4, B and C). These data indicate that Vps34 in TECs is required for a normal level of disease directed at a central nervous system autoantigen.

cTECs present increased abundance of CLIP-bound I-A^b complexes in the absence of Vps34

Surface levels and turnover rates of MHC class II on cTECs are critically important for positive selection of CD4$^+$ T cells (von

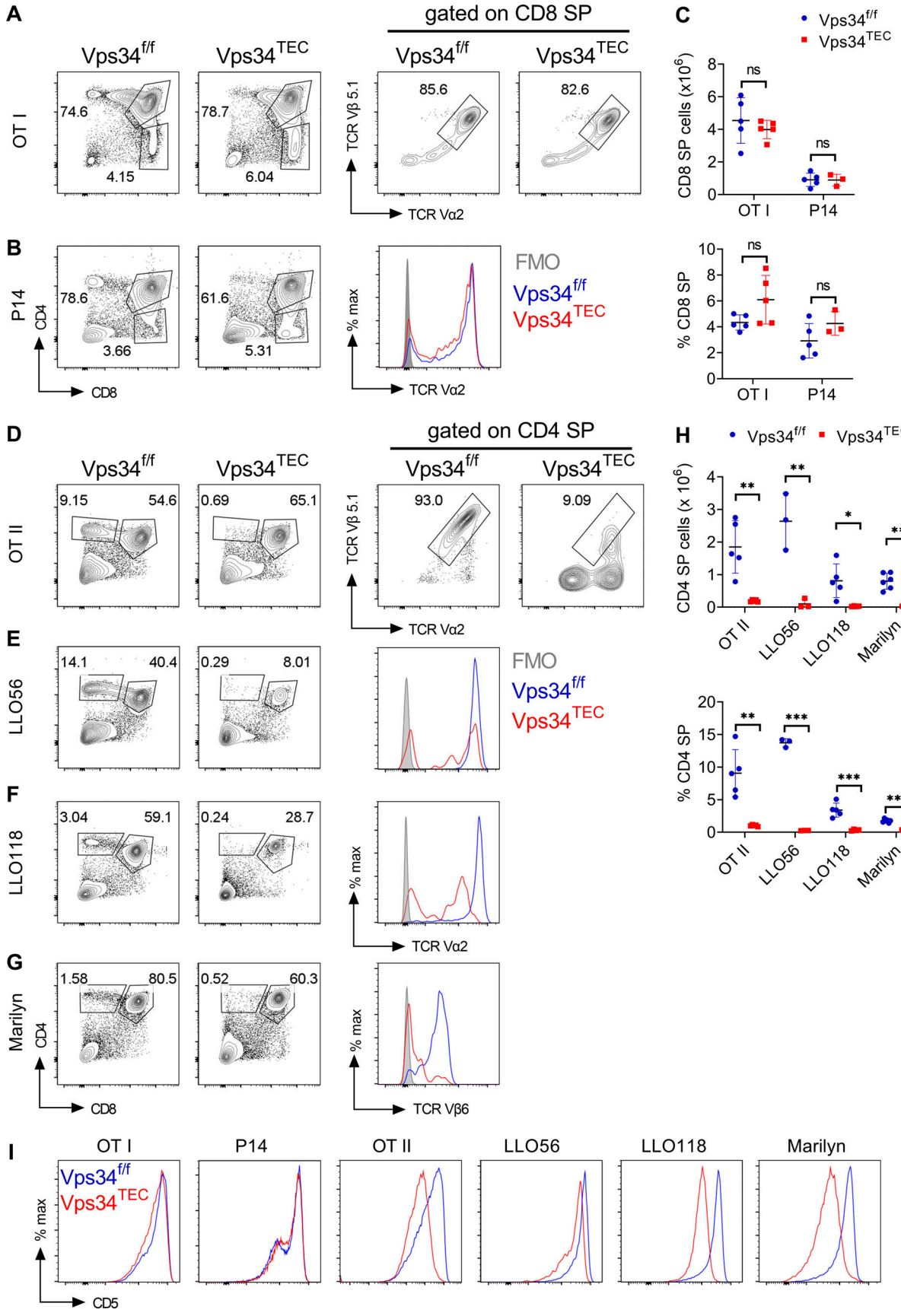

Figure 5. **Vps34 in TECs is critical for positive selection of MHC class II–restricted but not MHC class I–restricted transgenic TCRs.** Six separate TCR transgenes were introgressed into the Vps34^{TEC} strain and analyzed for positive selection compared with TCR transgenic Vps34$^{f/f}$ controls (see Table S1 for the

specificities of these TCRs). **(A–G)** Flow cytometric analysis of thymocytes for CD4 and CD8 expression from the following TCR transgenic lines: OTI (A), P14 (B), OTII (D), LLO56 (E), LLO118 (F), and Marilyn (females only; G). Representative flow plots or histograms show clonotypic TCR expression profiles of $Vps34^{f/f}$ (blue line), $Vps34^{TEC}$ (red line), and control staining (shaded gray) of the indicated cell populations. **(C)** Total cell number (top) and frequency (bottom) of CD8 SP thymocytes in the indicated MHC class I–restricted TCR transgenic lines. **(H)** Total cell number (top) and frequency (bottom) of CD4 SP thymocytes in the indicated MHC class II–restricted TCR transgenic lines. **(I)** Surface CD5 expression on DP thymocytes ($CD4^+CD8^+$) from the indicated mouse strains. Data signify the mean ± SD. Data are representative of at least two independent experiments with three to six biological replicates per genotype. Each data point represents a biological replicate. *, $P < 0.05$; **, $P < 0.01$; ***, $P < 0.001$; ns, not significant by unpaired *t* test. FMO, fluorescence minus one.

Rohrscheidt et al., 2016). Autophagy-related proteins including Vps34 have been implicated in regulating surface expression of MHC molecules (Van Kaer et al., 2019). However, we found no significant changes in the surface expression levels of either the MHC class I molecule K^b or the MHC class II molecule I-A^b on Vps34-deficient cTECs (Fig. 7, A and B). To investigate whether a particular MHC class II–bound peptide on cTECs was affected by loss of Vps34, we used a monoclonal antibody (15G4) that recognizes I-A^b when occupied by the invariant chain peptide derivative CLIP (class II–associated invariant chain peptide; Beers et al., 2005). After synthesis in the ER, MHC class II molecules contain CLIP in their peptide binding groove. In MHC class II compartments, the peptide editor DM promotes the exchange of CLIP for higher-affinity peptide. However, a fraction of class II molecules is presented at the surface while containing CLIP (Denzin et al., 2017). Indeed, we found that cTECs from $Vps34^{f/f}$ animals express CLIP-bound I-A^b molecules at levels above background staining of cTECs isolated from an MHC disparate strain (I-A^d-expressing BALB/c; Fig. 7 C). cTECs isolated from $Vps34^{TEC}$ mice expressed significantly increased levels of CLIP-bound I-A^b vs. WT controls. These findings indicate that Vps34 is required by cTECs to present normal surface levels of an endogenous self-peptide/MHC class II complex and suggest a role for Vps34 in generating the repertoire of self-peptides that is specialized for positive selection.

To analyze the contribution of Vps34 to vesicle trafficking in TECs, we used the mouse cTEC cell line C9 (Wertheimer et al., 2018). We deleted Vps34 in C9 cells using the CRISPR/Cas9 approach, generating stable control sgLacZ cells and Vps34-deficient sgVps34 cells. Efficient deletion of Vps34 in sgVps34 cells was confirmed by significant decrease in Vps34 protein expression (Fig. 7 D). Basal autophagy was disrupted in sgVps34 cells as evidenced by the accumulation of P62, a factor that targets cargo to autophagosomes and is itself degraded by autophagy. Previous studies report that disruption of Vps34 expression in vitro and in vivo causes a vacuolization phenotype associated with defects in endosomal trafficking (Bechtel et al., 2013; Jaber et al., 2016; Johnson et al., 2006). Examination of the cultures by light microscopy revealed that a significant proportion of Vps34-deficient cells accumulated numerous phase-lucent spherical cytoplasmic vacuoles (Fig. 7 E). Strikingly, H&E staining of thymic sections from neonates also revealed vacuolization caused by the absence of Vps34. To assess vesicle trafficking, we analyzed the maturation of the lysosomal protease cathepsin L, which is required by cTECs for efficient positive selection of $CD4^+$ T cells in vivo (Honey et al., 2002; Nakagawa et al., 1998). We found a significant decrease in the mature forms of cathepsin L, suggesting a significant abnormality in the ability of the lysosome to cleave cathepsin L (Fig. 7 D). We next considered that lysosomal alkalinization in Vps34-deficient cells may contribute to altered lysosomal protease activity and thus altered antigen processing. To determine whether Vps34 deficiency affects lysosomal pH, we stained C9 cells with LysoSensor Green DND-189, which accumulates in acidic organelles, where it increases its green fluorescence. Our results failed to show a significant difference in the relative acidity of lysosomes in sgVps34 cells compared with control sgLacZ cells (Fig. 7 F). However, in this assay, it remains possible that changes in total lysosomal content in Vps34-deficient cells could obscure differences in lysosomal pH.

Vps34 regulates positive selection in a canonical autophagy-independent mechanism

In addition to autophagy, Vps34 plays a role in endocytosis and vesicle trafficking (Backer, 2016), both of which can contribute to antigen presentation (Kondo et al., 2017). To investigate the role autophagy plays in the T cell selection phenotype observed in $Vps34^{TEC}$ mice, we generated mice with a TEC-specific deficiency of Atg5 ($Atg5^{TEC}$ mice), an essential component of the autophagy pathway (Levine and Kroemer, 2019), by crossing the Foxn1-Cre strain to mice with a floxed *Atg5* allele (Hara et al., 2006). We restricted our initial analysis to neonates for a better comparison with $Vps34^{TEC}$ mice. Consistent with a recent report in adult mice (Jain et al., 2018), Atg5 deficiency in TECs did not cause a detectable change in TEC frequency or cellularity (Fig. S5 A). Further, there was no change in subset ratios or numbers (Fig. S5 B). Consistent with a previous report using Atg5-deficient thymus grafts (Nedjic et al., 2008), we failed to detect any difference in the intrathymic development of the polyclonal repertoire in $Atg5^{TEC}$ mice (Fig. S5 C). To test if the autophagy pathway is necessary for positive selection of an MHC class II–restricted transgenic TCR that was dependent on Vps34 sufficiency in TECs, we investigated positive selection of OTII cells in $Atg5^{TEC}$ mice. We generated bone marrow chimeric animals by lethally irradiating either WT or $Atg5^{TEC}$ mice and transplanting bone marrow isolated from OTII transgenic donors. Our analysis revealed no significant change in the selection and development of OTII cells in $Atg5^{TEC}$ recipient mice (Fig. S5 D).

Radiation has been shown to induce autophagy (Chaurasia et al., 2016) and it is feasible that thymic recovery following radiation is compromised in the absence of Atg5, which may confound the interpretation of these results. Further, recent reports have highlighted the changes that occur in thymic selection from early life to adulthood (Dong et al., 2017; Smith et al., 2018). Therefore, for a more direct comparison, we analyzed positive selection of OTII cells in neonatal $Atg5^{TEC}$ mice by breeding in the OTII TCR transgene to $Atg5^{TEC}$ mice. Consistent with data from the chimera experiments, we found no alteration

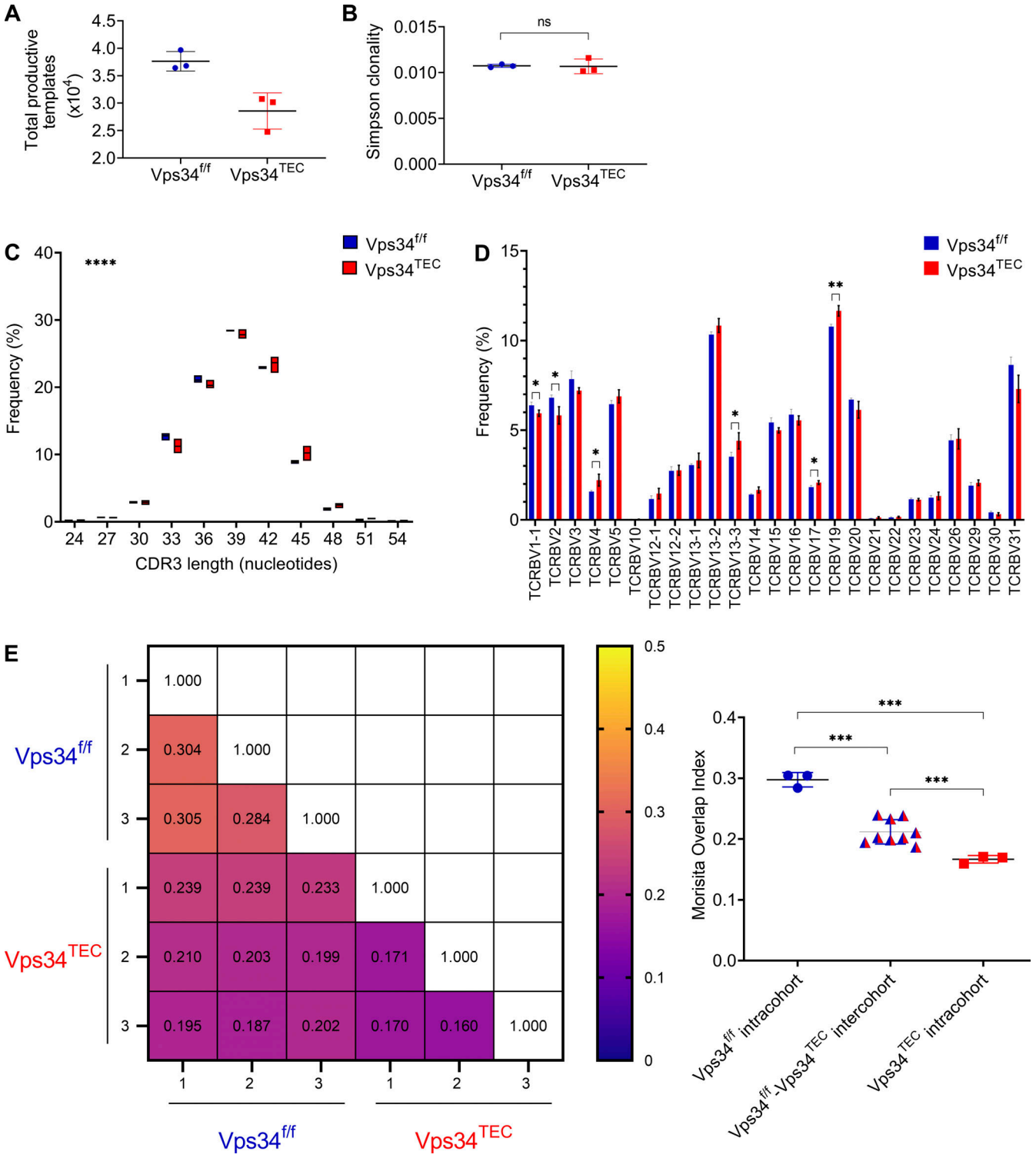

Figure 6. **TCRβ chains display altered gene usage and repertoire sharing in CD4 SP thymocytes of neonatal Vps34^{TEC} mice.** The somatically rearranged TCRβ CDR3 sequences were amplified from genomic DNA isolated from CD4 SP TCRβ$^+$ thymocytes flow sorted from 4- or 6-d-old Vps34$^{f/f}$ or Vps34^{TEC} mice (n = 3/genotype). **(A)** Numbers of productive TCR sequences. **(B)** Simpson clonality indexes of TCR repertoire diversity. **(C)** Distribution of CDR3 lengths (χ^2 test). **(D)** Distribution of TCR Vβ gene usage. **(E)** Heatmap of Morisita repertoire overlap across all samples. The graph represents the Morisita overlap index for each individual comparison organized by group. Data signify the mean ± SD. *, P < 0.05; **, P < 0.01; ***, P < 0.001; ****, P < 0.0001 by unpaired t test unless otherwise indicated.

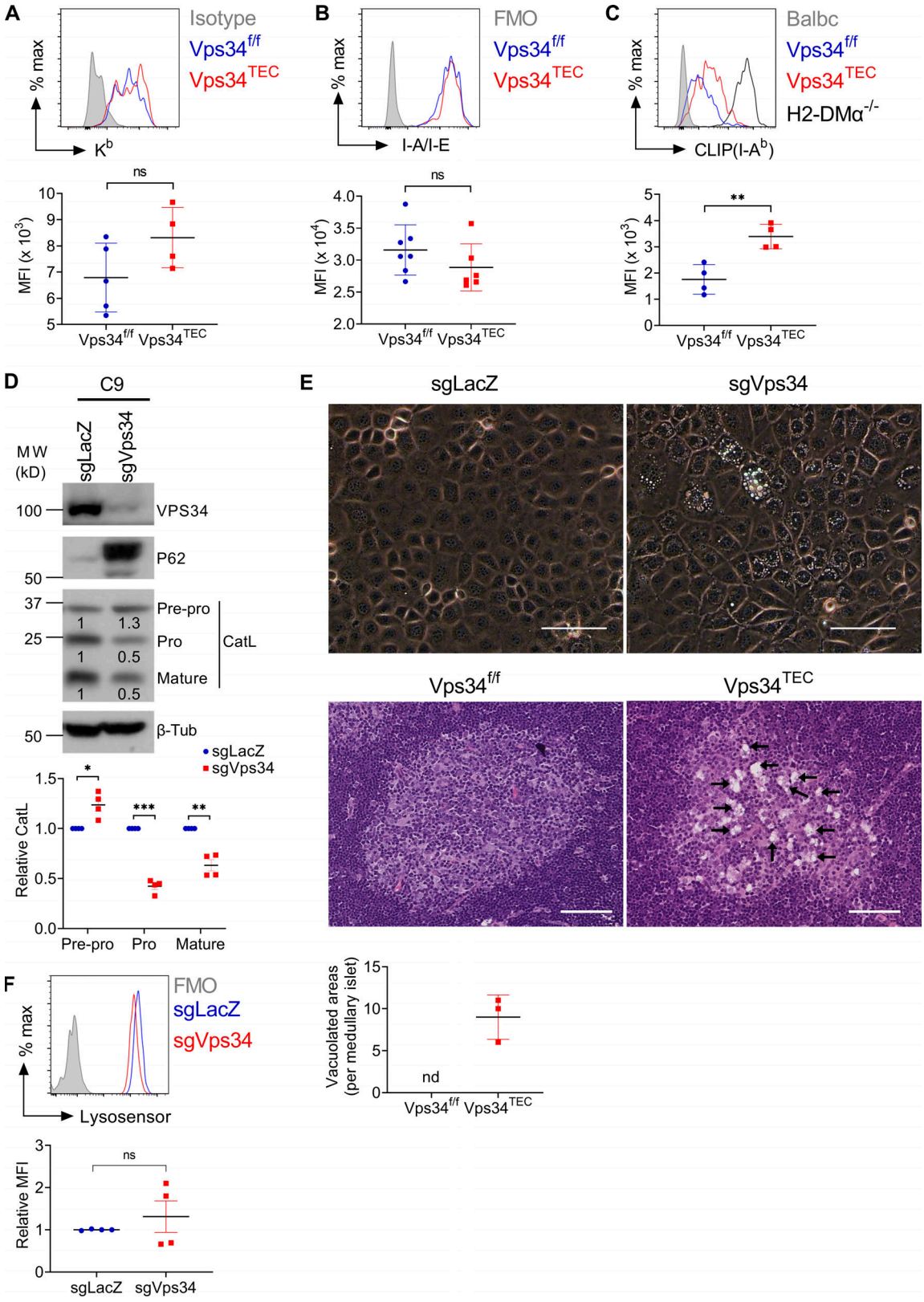

Figure 7. **cTECs present increased abundance of CLIP-bound I-A^b complexes in the absence of Vps34. (A–C)** cTECs (CD45$^-$EpCAM$^+$Ly-51$^+$) isolated from the indicated strains (isotype and FMO [fluorescence minus one] staining are from Vps34$^{f/f}$ isolated cells) were analyzed for (A) MHC class I (H-2K^b), (B) MHC class II (H-2I-A/I-E), or (C) CLIP-bound I-A^b expression by flow cytometry. Data are representative of at least two independent experiments (n = 4–7 per genotype). **(D)** Protein isolated from control and Vps34-deleted C9 cells were analyzed by Western blot for markers of autophagy and vesicle trafficking. β-Tubulin was used as loading control. The graph represents the relative densities of pre-pro-cathepsin L, pro-cathepsin L, and mature cathepsin L bands (CatL) between sgLacZ and sgVps34. Data are representative of two independent experiments. **(E)** Light micrograph of live control (sgLacZ) and Vps34-deleted

(sgVps34) C9 cells (top, scale bar = 100 µm). Thymus tissue sections from 3-d-old $Vps34^{f/f}$ or $Vps34^{TEC}$ mice stained with H&E (bottom, scale bar = 75 µm). Arrows highlight areas of significant vacuolization. The graph represents the number of vacuolated areas per medullary islet. Data are from one randomly selected medullary islet from three independent biological replicates of each genotype. **(F)** sgVps34 and sgLacZ cells were stained with Lysosensor green probe and then analyzed by flow cytometry. The graph represents relative mean fluorescence intensity (MFI) of Lysosensor green. Data are representative of two independent experiments. All data signify the mean ± SD. *, P < 0.05; **, P < 0.01; ***, P < 0.001; ns, not significant; nd, none detected by unpaired *t* test. Source data are available for this figure: SourceData F7.

in OTII cell-positive selection between $Atg5^{TEC}$ mice and their littermate controls (Fig. S5 E). Collectively, our data show that Atg5-dependent autophagy is not required by TECs to positively select a TCR that is dependent on Vps34-mediated cell processes in TECs. Therefore, we propose that Vps34 in TECs regulates positive selection in a canonical autophagy-independent mechanism.

Discussion

The class III PI3K Vps34 plays key roles in autophagy, endocytosis, and vesicle trafficking (Bilanges et al., 2019), processes that control the presentation of self-antigens by TECs to developing thymocytes (Klein et al., 2014). Here we analyzed mice with a TEC-specific *Vps34* gene ablation. $Vps34^{TEC}$ mice exhibited a progressive loss in thymocyte cellularity that led to T cell lymphopenia in adult animals. The gradual loss in thymopoiesis was preceded by a reduction in TEC cellularity, suggesting that the eventual loss of DP thymocytes is likely due to insufficient TEC numbers. Using the Foxn1 promoter to drive Cre recombinase expression for gene targeting, Vps34 is likely deleted in TECs starting at the initiation of thymic organogenesis (Martinez-Ruiz et al., 2022), which raises the possibility that the observed alterations in TEC cellularity are due to loss of TEPCs. Our results with a genetic system to inducibly target *Vps34* ablation in postnatal thymi indicate that TECs continue to require Vps34 for their homeostasis and to facilitate thymopoiesis after mature TECs have completed their development. TEC-specific loss of Vps34 also caused significant alterations in thymic morphology. While conditional loss of Vps34 reduced the cellularity of both cTECs and mTECs, the latter TEC subset was relatively more profoundly impacted. However, at present it is unclear if the deficiency in the mTEC compartment is a result of a defect in the capacity of TEC precursors to develop into mTECs, a failure of committed mTECs to expand, or increased mTEC death. We observed a significant decrease in $Ki67^+$ mTECs in $Vps34^{TEC}$ mice, indicating that a reduction in proliferating mTECs may partially explain these defects. However, it is unclear whether there is an mTEC-intrinsic requirement for cell proliferation. Positively selected $CD4^+$ T cells supply pro-expansion signals to mTECs via RANK and CD40 interactions (Akiyama et al., 2008; Hikosaka et al., 2008). Therefore, TEC-specific loss of Vps34 may have secondary effects on mTEC cellularity driven by altered CD4 SP/mTEC crosstalk. Collectively, our data identify a critical role for Vps34 in maintaining thymic function. These findings also provide a rationale for targeting Vps34 activity in scenarios where enhancement of thymic function may be desired, such as during aging, recovery from radiation therapy or chemotherapy, T cell reconstitution following stem cell transplantation, and infection or inflammation that compromise T cell thymic output.

cTECs rely on unique antigen-processing machinery to produce a repertoire of self-antigens specialized for T cell positive selection (Kondo et al., 2017). While in most APCs, antigens presented on MHC class II are derived from extracellular sources, cTECs present self-antigens derived from intracellular origins (Klein et al., 2014). Here, we propose that TECs require Vps34-mediated cellular processes to produce a diverse collection of self-peptides needed for the development and positive selection of a broad $CD4^+$ T cell repertoire. Our finding that Vps34-deficient cTECs express increased surface levels of CLIP-bound MHC class II molecules provides indirect support for this possibility.

Our results show that loss of Vps34 in TECs causes defects in the development of $CD4^+$ T cells in neonatal mice. Vps34-deficient TECs were also unable to positively select MHC class II–restricted transgenic TCRs but retained their capacity to select MHC class I–restricted transgenic TCRs, providing further evidence that Vps34 is crucial in processing antigens for presentation by MHC class II but not MHC class I in cTECs. Because MHC class I–restricted TCRs were selected in $Vps34^{TEC}$ mice, it is unlikely that the defect in $CD4^+$ T cell development in neonatal mice is due to TEC dysfunction other than MHC presentation, such as producing and secreting factors necessary for recruiting lymphoid progenitors, T cell lineage commitment, or T cell lineage expansion before positive selection.

Previous reports analyzing the TCR repertoire of mice with targeted mutations that significantly reduce the variety of self-peptides bound to MHC class II molecules have provided evidence that positive selection on a restricted collection of self-peptides is sufficient to select for a broad but distinct $CD4^+$ TCR repertoire (Pacholczyk et al., 2006; Wong et al., 2007). Consistent with these findings, we found a close degree of clonality maintained in the $CD4^+$ TCR repertoire in $Vps34^{TEC}$ mice compared with control mice. However, we found significantly reduced clonal sharing and altered TCR Vβ gene segment usage in $CD4^+$ T cells in the absence of Vps34 in TECs. These results indicate that Vps34-mediated cellular processes in TECs are crucial for shaping the TCR repertoire in $CD4^+$ T cells. Although the defect in the development of $CD4^+$ T cells expressing MHC class II–restricted transgenic TCRs illustrates a role for Vps34 in the positive selection of $CD4^+$ T cells, we cannot exclude that the TCR sequencing data of the polyclonal repertoire is influenced by alterations in negative selection in $Vps34^{TEC}$ mice.

A previous report using Atg5-deficient thymic grafts argued that autophagy promotes positive selection of the $CD4^+$ TCR repertoire by providing selecting ligands bound to MHC class II

molecules (Nedjic et al., 2008). In that system, more modest effects in positive selection using transgenic TCR lines were observed compared with the positive selection defects of MHC class II–restricted transgenic TCRs reported here in Vps34^{TEC} mice. Importantly, we did not observe significant changes in positive selection of OTII cells in mice with a TEC-specific Atg5 deficiency. Yet we found a near-complete block in positive selection of OTII cells in Vps34^{TEC} mice. Given these observations, along with a profound block in autophagic flux in Vps34-deficient TECs, it is unlikely that the observed alterations in positive selection of CD4$^+$ T cells in Vps34^{TEC} mice are due solely to a loss in autophagy. Nevertheless, it remains possible that Atg5-independent autophagy plays a role in the defective CD4$^+$ T cell selection phenotype observed in Vps34^{TEC} mice. Atg5-independent autophagy has been reported in some studies (Honda et al., 2014; Ma et al., 2015; Nishida et al., 2009). Furthermore, a Vps34-dependent noncanonical form of autophagy, termed LC3-associated phagocytosis (LAP), has been described (Martinez et al., 2015). LAP supports antigen presentation in mouse macrophages by regulating the processing of endocytosed antigens for presentation to MHC class II–restricted CD4$^+$ T cells (Munz, 2018). Importantly, mice that are deficient in LAP due to genetic targeting of Rubicon do not display defects in T cell development (Martinez et al., 2016). Therefore, it is unlikely that Vps34 contributes to antigen presentation by TECs via LAP. Finally, a recent study analyzed T cell selection in thymic grafts deficient in Lamp2 (Rodrigues et al., 2022), a lysosomal protein that has been implicated in chaperone-mediated autophagy, macroautophagy, and lysosomal function (Kaushik and Cuervo, 2018; Sudhakar et al., 2020). Lamp2 was shown to be necessary for cTEC autophagy, normal cathepsin L activity, and CD4 but not CD8 T cell selection. Considering the similarities of this phenotype with the defects reported here in Vps34^{TEC} mice, it is tempting to speculate that Lamp2 and Vps34 modulate TEC cell function by similar mechanisms.

We propose that the thymic selection defect in Vps34^{TEC} mice is caused by defects in endocytosis and/or vesicle trafficking, rather than canonical autophagy. We found that loss of Vps34 in TECs did not alter levels of MHC class II molecules on the surface of cTECs, indicating that endocytic turnover or recycling of peptide-MHC class II molecules is not the underlying cause for the defect in positive selection of CD4 T cells. However, we found an increase in the abundance of surface MHC class II molecules occupied by the invariant chain derivative peptide CLIP, indicating quantitative alterations in the repertoire of self-peptides bound to MHC class II molecules. Previous reports have identified vesicle trafficking dependent on Vps34 catalytic activity as necessary for the endosomal processing of the protease cathepsin D into its active mature form (Jaber et al., 2016; Reifler et al., 2014; Ronan et al., 2014; Row et al., 2001). Our analysis of Vps34-deficient C9 cells provides evidence that steady-state levels of mature cathepsin L require Vps34 in cTECs. Strikingly, many of the T cell defects observed in cathepsin L knockout mice resemble those seen in Vps34^{TEC} mice, including altered CD4$^+$ T cell selection and increased abundance of CLIP-bound MHC class II molecules on cTECs (Honey et al., 2002; Nakagawa et al., 1998). Taken together, our findings provide evidence that cTECs require Vps34 for the generation of the self-peptide/MHC class II repertoire in a mechanism involving Vps34-dependent proteolytic activity, but likely not autophagy-mediated delivery of antigens to MHC class II–containing compartments.

In summary, our present study provides new insights into the mechanisms governing the processing and presentation of self-antigens by cTECs required for thymic selection of a broad CD4$^+$ T cell repertoire. These findings could have practical implications for restoring or rejuvenating thymic function in situations of defective thymopoiesis.

Materials and methods

Mice

All mouse strains used, their genetic background, and their sources are outlined in Table S2. TEC-specific deletion of *Vps34* and *Atg5* was achieved by crossing Vps34$^{f/f}$ and Atg5$^{f/f}$ mice with Foxn1-Cre mice. Cre$^-$ littermates were used as controls in all experiments except the bone marrow chimera experiments represented in Fig. S5 D. Newborn to 10-wk-old animals of both sexes were used in this study. All breeder and experimental mice were housed under specific pathogen–free conditions in compliance with guidelines from the Institutional Animal Care and Use Committee at Vanderbilt University.

Flow cytometric analysis

T cells from thymi, lymph nodes, and spleens were obtained by mashing the organ through a 70-µm cell strainer (22-363-548; Thermo Fisher Scientific) and suspended in FACS buffer (PBS containing 2% FBS). Cells were incubated with conjugated monoclonal antibodies against mouse CD4 (Tonbo), CD8α (Tonbo), CD3ε (BioLegend), CD44 (Tonbo), CD62L (BD Biosciences), CD69 (BD Biosciences), TCRβ (Tonbo), CD24 (BD Biosciences), CD25 (Tonbo), cKit (eBioscience), CD5 (BioLegend), TCR Vα2 (BioLegend), TCR Vβ5.1 (BioLegend), and/or TCR V β 6 (BD Biosciences).

For iNKT cell and MAIT cell analysis, thymi were processed as above. Cells were incubated with monoclonal antibody against mouse CD3ε (BioLegend), PBS57/CD1d-tetramer conjugated to allophycocyanin (APC), and 5-OP-RU/MR1-tetramer conjugated to Pacific blue. Both tetramers were obtained from the National Institutes of Health Tetramer Core Facility at Emory University (Atlanta, GA).

For TEC analysis, thymi were dissected and digested in 1 mg/ml collagenase/dispase (Roche) and passed through a 100-µm mesh to remove debris. Monoclonal antibodies against mouse CD45.2 (Tonbo), EpCam (BioLegend), Ly51 (eBioscience), CD80 (BD Biosciences), K^b (BD Biosciences), I-A^b plus CLIP (15G4; Santa Cruz), mouse IgG1 (eBioscience) and I-A/I-E (eBioscience), Sca-1 (eBioscience), Itga6 (BioLegend), and the UEA1 lectin (Vector Labs) were used in the TEC analysis.

For intracellular staining, TECs were processed and stained for extracellular markers as described. Cells were fixed and permeabilized using FOXP3 fix/perm buffer kit (BioLegend) overnight at 4°C. Cells were then incubated with a monoclonal antibody against Ki67 (eBioscience). Cells were washed and then

analyzed. Flow cytometric analyses were performed using a Canto II or 4 laser Fortessa (BD Biosciences) flow cytometer. The acquired data were analyzed using FlowJo software (v10.0.7; TreeStar).

FACS

Cells were stained as described for flow cytometry. ~1.1 × 10^5 TCRβ^{hi}, CD4$^+$CD8$^-$ thymocytes were sorted into cold Hepes buffer (PBS with 2% FBS and 0.025 M Hepes) and immediately used for genomic DNA isolation. Sorting was performed using a FACS Aria III (BD Biosciences) flow cytometer.

Immunofluorescence and histology

For cryosectioning, thymi were snap-frozen on dry ice and stored at −80°C. Tissues were sectioned at 8-µm thickness and fixed in ice-cold acetone for 5 min. Tissues were rinsed with PBS, blocked with 10% donkey serum in PBS for 30 min at room temperature, and incubated with the primary antibody anti-Keratin 5 (Abcam) or biotin-labeled UEA-1 lectin (Vector Labs) overnight at 4°C. Secondary detection was performed with goat anti-rabbit IgG (Jackson ImmunoResearch) and Streptavidin-Cy3 (Vector Labs). Sections were examined by fluorescent microscopy using a Zeiss LSM 710 confocal microscope.

For paraffin sectioning, tissues were collected and fixed in 10% paraformaldehyde for formalin overnight. Tissues were dehydrated through an ethanol series and embedded in paraffin wax using standard procedures. Sections (8 µm) were cut and rinsed in xylene before rehydration through a reverse ethanol series. H&E staining was performed on paraffin sections using standard procedures; sections were then imaged on a Nikon AZ 100M wide-field microscope.

Thymus grafts

Thymic lobes were dissected from newborn Rosa26-CreER^{T2}; Vps34$^{f/f}$ or Vps34$^{f/f}$ mice and placed in ice-cold PBS. Thymi were separated into single lobes, and connective tissue was removed. A single lobe was transplanted under the kidney capsule of each 6-wk-old male C57BL/6 recipient as described (Jain et al., 2017). Grafts were allowed to reconstitute for 3 wk, and mice were orally gavaged with 3 mg of tamoxifen (Sigma-Aldrich) in peanut oil or vehicle for three alternate days and analyzed 3 wk after the final dose.

TCR sequencing and analysis

Sample preparation

Genomic DNA was prepared from CD4$^+$CD8$^-$ TCRβ^{hi} thymocytes sorted from 4- or 6-d-old mice using a standard Qiagen DNA extraction kit according to the manufacturer's instructions. Library preparation and sequencing sample data were generated using the immunoSEQ Assay (Adaptive Biotechnologies). The somatically rearranged mouse TCRβ CDR3 regions were amplified from genomic DNA using a two-step, amplification bias-controlled multiplex PCR approach. The first PCR consisted of forward and reverse amplification primers specific for every known V and J gene segment and amplified the hypervariable CDR3 of the immune receptor locus. The second PCR added a proprietary barcode sequence and Illumina adapter sequences. In addition, reference gene primers were included in the PCR reaction to quantify total sequenceable nucleated cells and to accurately measure the fraction of T cells in each sample. CDR3 and reference gene libraries were sequenced on an Illumina instrument according to the manufacturer's instructions.

Data analysis

Raw sequence reads were demultiplexed according to Adaptive's proprietary barcode sequences. Demultiplexed reads were then further processed to remove adapter and primer sequences and to identify and remove primer dimers, germline, and other contaminant sequences. The filtered data were clustered using both the relative frequency ratio between similar clones and a modified nearest-neighbor algorithm, to merge closely related sequences to correct for technical errors introduced through PCR and sequencing. The resulting sequences were sufficient to allow annotation of the V, D, and J genes and the N1 and N2 regions constituting each unique CDR3 and the translation of the encoded CDR3 amino acid sequence. Gene definitions were based on annotation in accordance with the International Immunogenetics Information System database (http://www.imgt.org). The set of observed biological TCRβ CDR3 sequences was normalized to correct for residual multiplex PCR amplification bias and quantified against a set of synthetic TCRβ CDR3 sequence analogues. Data were analyzed using the immunoSEQ Analyzer toolset. Data were imported into GraphPad Prism 6.0 for statistical analyses and graph generation.

Induction and evaluation of active EAE

6- to 8-wk-old animals were used for EAE induction, as described (Miller et al., 2010). Under isoflurane anesthesia, the animals were subcutaneously injected at two sites into the flank with 200 µl of 1 mg/ml $MOG_{35–55}$ (MEVGWYRSPFSRVVHLYRNGK) peptide (Biomatik) emulsified in Freund's complete adjuvant (2 mg/ml *Mycobacterium tuberculosis* extract H37Ra in incomplete Freund's adjuvant [263910; BD Bioscience]). Immediately after immunization and 48 h later, all mice received 400 ng of pertussis toxin (516560; Calbiochem) by i.p. injection. Mice were scored daily in a blinded manner according to the following scale: 0, no clinical signs; 0.5, partially limp tail; 1, paralyzed tail; 1.5, paralyzed tail and hind leg inhibition; 2, loss in coordinated movement, hind limb paresis; 2.5, one hind limb paralyzed; 3; both hind limbs paralyzed; 3.5, hind limbs paralyzed, weakness in forelimbs; 4, forelimbs paralyzed; 5, moribund.

TEC culture

C9 cells (Wertheimer et al., 2018; kindly provided by Dr. M. van den Brink from Memorial Sloan Kettering Cancer Center, New York, NY) were cultured in DMEM supplemented with 10% (v/v) FBS (HyClone Fetal Clone III), 100 units/ml penicillin, and 100 µg/ml streptomycin.

CRISPR-Cas9 editing of Vps34 in C9 cells

For excision of the *Vps34* gene, we used a lentivirus harboring either lentiCRISPR v2 empty vector (#52961; Addgene) or lentiCRISPR v2 sgVps34. We amplified lentiviruses as described

(Song et al., 2014). Parental C9 cells were transfected with the respective virus to produce control sgLacZ cells and stable Vps34-deficient sgVps34 cells. gRNA sequence for Vps34 was 5′-TCTCGTAGCATGTTTCGCCA-3′.

Western blotting

C9 cells were lysed in radioimmunoprecipitation assay buffer (Sigma-Aldrich) containing a cocktail of protease inhibitors (Roche) with brief sonication. Total proteins (50 µg) were separated on SDS-PAGE gels, transferred onto PVDF membranes, and incubated with primary antibodies. Secondary antibodies were subsequently applied and proteins were detected with ECL substrate (Clarity; Bio-Rad) or using an LI-COR Odyssey Infrared Imaging System.

Lysosomal pH measurement

sgLacZ and sgVps34 C9 cells were trypsinized and loaded with LysoSensor Green DND-189 (1 mM; Thermo Fisher Scientific) in PBS buffer for 15 min at 37°C. Cells were washed twice with PBS and immediately analyzed by flow cytometry. LysoSensor Green DND-189 dye accumulates in acidic organelles and becomes more fluorescent with decreasing pH. Relative mean fluorescence intensity in the GFP channel was used to compare lysosomal pH.

Generation of bone marrow chimeras

Recipient mice were lethally irradiated (1,000 cGy) and 6 h later injected with ∼10^7 bone marrow cells derived from OTII mice. Mice were used for experiments at 5–6 wk after injection of bone marrow cells.

Statistical analysis

Statistical analysis was performed with Prism 6.0 (GraphPad Software). Data are presented as mean ± SD. *N* was ≥3 for each genotype in each experiment, as indicated in the text and/or figure legends. Comparisons between two groups were made using two-tailed Student's *t* test; $P < 0.05$ was considered significant.

EAE

EAE clinical scores and disease incidence were analyzed using ANOVA and Kaplan–Meier curves by log-rank test. Peak disease score was analyzed by two-tailed Student's *t* test. $P < 0.05$ was considered significant.

TCR sequencing

Clonality, gene usage, and overlap comparisons were analyzed by two-tailed Student's *t* test. CDR3 length was analyzed by χ^2 test (Miqueu et al., 2007). $P < 0.05$ was considered significant.

Online supplemental material

Fig. S1 shows $Vps34^{TEC}$ phenotype related to Figs. 1 and 2. Fig. S2 shows DN thymocyte development, splenic T cell phenotype, and nonconventional T cell development in neonatal $Vps34^{TEC}$ mice. Fig. S3 shows splenic phenotype in 1-wk-old TCR^{Tg} $Vps34^{TEC}$ mice. Fig. S4 shows EAE disease severity and incidence in adult $Vps34^{TEC}$ mice. Fig. S5 shows TEC phenotype and T cell selection in neonatal $Atg5^{TEC}$ mice. Table S1 describes the specificities of TCR transgenic lines used in Fig. 5. Table S2 outlines information pertaining to mouse strains used in the present study.

Data availability

The datasets generated during the current study are available from the corresponding author upon request.

Acknowledgments

The authors thank Drs. Mark Boothby (Vanderbilt University School of Medicine, Nashville, TN), Mark Anderson (University of California, San Francisco, San Francisco, CA), Paul Allen (Washington University School of Medicine, St. Louis, MO), Akiko Iwasaki (Yale School of Medicine, New Haven, CT), Maria-Luisa Alegre (The University of Chicago, Chicago, IL), and Marcel van den Brink (Memorial Sloan Kettering Cancer Center, New York, NY) for sharing valuable reagents. We also thank Dr. Vrajesh Parekh (Vanderbilt University School of Medicine, Nashville, TN) for help with some of the mouse crosses. We thank the National Institutes of Health tetramer core at Emory University for the PBS57/CD1d, 6-FP/MR1, and 5-OP-RU/MR1 tetramers.

This work was supported by grants from the National Institutes of Health (R01DK104817 and R01AI139046 to L.V. Kaer), the American Heart Association (19TPA34910078 to L.V. Kaer), and Veterans Affairs Merit (I01BX001444 to S. Joyce) and Research Career Scientist (IK6BX004595 to S. Joyce) awards. J.L. Postoak was supported by predoctoral National Institutes of Health training grants (T32HL069765 and T32AR059039). The study used the following core resources at Vanderbilt University Medical Center: Cell Imaging Shared Resource (supported by National Institutes of Health grants P30CA068485, P30DK058404, and P30DK020593), Digital Histology Shared Resource, Translational Pathology Shared Resource (supported by National Institutes of Health grant P30CA068485), and Flow Cytometry Shared Resource (supported by National Institutes of Health grants P30CA068485, P30DK058404, and P30DK020593).

Author contributions: Conceived and designed the experiments: J.L. Postoak, N.R. Manley, L.V. Kaer. Performed the experiments: J.L. Postoak, W. Song, G. Yang, C.E. Saffold, L. Wu. Analyzed the data: J.L. Postoak, X. Guo, S. Xiao, N.R. Manley, L.V. Kaer. Contributed reagents/materials/analysis tools: J. Zhang, S. Joyce, N.R. Manley.

Disclosures: L. Van Kaer reported "I am a member of the scientific advisory board of Isu Abxis Co., Ltd. (South Korea), for which I get financial compensation. The company focuses on the development of antibody-mediated treatment for cancer and rare diseases. The work at the company is not directly related to this publication." No other disclosures were reported.

Submitted: 28 December 2021
Revised: 22 June 2022
Accepted: 3 August 2022

References

Akiyama, T., Y. Shimo, H. Yanai, J. Qin, D. Ohshima, Y. Maruyama, Y. Asaumi, J. Kitazawa, H. Takayanagi, J.M. Penninger, et al. 2008. The tumor necrosis factor family receptors RANK and CD40 cooperatively establish the thymic medullary microenvironment and self-tolerance. *Immunity*. 29:423–437. https://doi.org/10.1016/j.immuni.2008.06.015

Azzam, H.S., A. Grinberg, K. Lui, H. Shen, E.W. Shores, and P.E. Love. 1998. CD5 expression is developmentally regulated by T cell receptor (TCR) signals and TCR avidity. *J. Exp. Med.* 188:2301–2311. https://doi.org/10.1084/jem.188.12.2301

Backer, J.M. 2016. The intricate regulation and complex functions of the Class III phosphoinositide 3-kinase Vps34. *Biochem. J.* 473:2251–2271. https://doi.org/10.1042/BCJ20160170

Baran-Gale, J., M.D. Morgan, S. Maio, F. Dhalla, I. Calvo-Asensio, M.E. Deadman, A.E. Handel, A. Maynard, S. Chen, F. Green, et al. 2020. Ageing compromises mouse thymus function and remodels epithelial cell differentiation. *Elife*. 9:e56221. https://doi.org/10.7554/eLife.56221

Barthlott, T., H. Kohler, and K. Eichmann. 1997. Asynchronous coreceptor downregulation after positive thymic selection: Prolonged maintenance of the double positive state in CD8 lineage differentiation due to sustained biosynthesis of the CD4 coreceptor. *J. Exp. Med.* 185:357–362. https://doi.org/10.1084/jem.185.2.357

Bechtel, W., M. Helmstadter, J. Balica, B. Hartleben, B. Kiefer, F. Hrnjic, C. Schell, O. Kretz, S. Liu, F. Geist, et al. 2013. Vps34 deficiency reveals the importance of endocytosis for podocyte homeostasis. *J. Am. Soc. Nephrol.* 24:727–743. https://doi.org/10.1681/ASN.2012070700

Beers, C., A. Burich, M.J. Kleijmeer, J.M. Griffith, P. Wong, and A.Y. Rudensky. 2005. Cathepsin S controls MHC class II-mediated antigen presentation by epithelial cells in vivo. *J. Immunol.* 174:1205–1212. https://doi.org/10.4049/jimmunol.174.3.1205

Benlagha, K., D.G. Wei, J. Veiga, L. Teyton, and A. Bendelac. 2005. Characterization of the early stages of thymic NKT cell development. *J. Exp. Med.* 202:485–492. https://doi.org/10.1084/jem.20050456

Bilanges, B., Y. Posor, and B. Vanhaesebroeck. 2019. PI3K isoforms in cell signalling and vesicle trafficking. *Nat. Rev. Mol. Cell Biol.* 20:515–534. https://doi.org/10.1038/s41580-019-0129-z

Boukhalfa, A., A.C. Nascimbeni, D. Ramel, N. Dupont, E. Hirsch, S. Gayral, M. Laffargue, P. Codogno, and E. Morel. 2020. PI3KC2α-dependent and VPS34-independent generation of PI3P controls primary cilium-mediated autophagy in response to shear stress. *Nat. Commun.* 11:294. https://doi.org/10.1038/s41467-019-14086-1

Chaurasia, M., A.N. Bhatt, A. Das, B.S. Dwarakanath, and K. Sharma. 2016. Radiation-induced autophagy: Mechanisms and consequences. *Free Radic. Res.* 50:273–290. https://doi.org/10.3109/10715762.2015.1129534

Cowan, J.E., S.M. Parnell, K. Nakamura, J.H. Caamano, P.J.L. Lane, E.J. Jenkinson, W.E. Jenkinson, and G. Anderson. 2013. The thymic medulla is required for Foxp3$^+$ regulatory but not conventional CD4$^+$ thymocyte development. *J. Exp. Med.* 210:675–681. https://doi.org/10.1084/jem.20122070

Denzin, L.K., A.A. Khan, F. Virdis, J. Wilks, M. Kane, H.A. Beilinson, S. Dikiy, L.K. Case, D. Roopenian, M. Witkowski, et al. 2017. Neutralizing antibody responses to viral infections are linked to the non-classical MHC class II gene H2-Ob. *Immunity*. 47:310–322.e7. https://doi.org/10.1016/j.immuni.2017.07.013

Dong, M., P. Artusa, S.A. Kelly, M. Fournier, T.A. Baldwin, J.N. Mandl, and H.J. Melichar. 2017. Alterations in the thymic selection threshold skew the self-reactivity of the TCR repertoire in neonates. *J. Immunol.* 199:965–973. https://doi.org/10.4049/jimmunol.1602137

Galluzzi, L., and D.R. Green. 2019. Autophagy-independent functions of the autophagy machinery. *Cell*. 177:1682–1699. https://doi.org/10.1016/j.cell.2019.05.026

Gascoigne, N.R.J., V. Rybakin, O. Acuto, and J. Brzostek. 2016. TCR signal strength and T cell development. *Annu. Rev. Cell Dev. Biol.* 32:327–348. https://doi.org/10.1146/annurev-cellbio-111315-125324

Gordon, J., S. Xiao, B. Hughes 3rd, D.M. Su, S.P. Navarre, B.G. Condie, and N.R. Manley. 2007. Specific expression of lacZ and cre recombinase in fetal thymic epithelial cells by multiplex gene targeting at the Foxn1 locus. *BMC Dev. Biol.* 7:69. https://doi.org/10.1186/1471-213X-7-69

Han, J., and J.C. Zuniga-Pflucker. 2021. A 2020 view of thymus stromal cells in T cell development. *J. Immunol.* 206:249–256. https://doi.org/10.4049/jimmunol.2000889

Hara, T., K. Nakamura, M. Matsui, A. Yamamoto, Y. Nakahara, R. Suzuki-Migishima, M. Yokoyama, K. Mishima, I. Saito, H. Okano, and N. Mizushima. 2006. Suppression of basal autophagy in neural cells causes neurodegenerative disease in mice. *Nature*. 441:885–889. https://doi.org/10.1038/nature04724

Hikosaka, Y., T. Nitta, I. Ohigashi, K. Yano, N. Ishimaru, Y. Hayashi, M. Matsumoto, K. Matsuo, J.M. Penninger, H. Takayanagi, et al. 2008. The cytokine RANKL produced by positively selected thymocytes fosters medullary thymic epithelial cells that express autoimmune regulator. *Immunity*. 29:438–450. https://doi.org/10.1016/j.immuni.2008.06.018

Honda, S., S. Arakawa, Y. Nishida, H. Yamaguchi, E. Ishii, and S. Shimizu. 2014. Ulk1-mediated Atg5-independent macroautophagy mediates elimination of mitochondria from embryonic reticulocytes. *Nat. Commun.* 5:4004. https://doi.org/10.1038/ncomms5004

Honey, K., T. Nakagawa, C. Peters, and A. Rudensky. 2002. Cathepsin L regulates CD4$^+$ T cell selection independently of its effect on invariant chain: A role in the generation of positively selecting peptide ligands. *J. Exp. Med.* 195:1349–1358. https://doi.org/10.1084/jem.20011904

Jaber, N., Z. Dou, J.S. Chen, J. Catanzaro, Y.P. Jiang, L.M. Ballou, E. Selinger, X. Ouyang, R.Z. Lin, J. Zhang, and W.X. Zong. 2012. Class III PI3K Vps34 plays an essential role in autophagy and in heart and liver function. *Proc. Natl. Acad. Sci. USA*. 109:2003–2008. https://doi.org/10.1073/pnas.1112848109

Jaber, N., N. Mohd-Naim, Z. Wang, J.L. DeLeon, S. Kim, H. Zhong, N. Sheshadri, Z. Dou, A.L. Edinger, G. Du, et al. 2016. Vps34 regulates Rab7 and late endocytic trafficking through recruitment of the GTPase-activating protein armus. *J. Cell Sci.* 129:4424–4435. https://doi.org/10.1242/jcs.192260

Jain, R., J.D. Mintern, I. Tan, G. Dewson, A. Strasser, and D.H.D. Gray. 2018. How do thymic epithelial cells die? *Cell Death Differ.* 25:1002–1004. https://doi.org/10.1038/s41418-018-0093-8

Jain, R., J.M. Sheridan, A. Policheni, M. Heinlein, L.C. Gandolfo, G. Dewson, G.K. Smyth, S.N. Sansom, N.Y. Fu, J.E. Visvader, et al. 2017. A critical epithelial survival axis regulated by MCL-1 maintains thymic function in mice. *Blood*. 130:2504–2515. https://doi.org/10.1182/blood-2017-03-771576

Johnson, E.E., J.H. Overmeyer, W.T. Gunning, and W.A. Maltese. 2006. Gene silencing reveals a specific function of hVps34 phosphatidylinositol 3-kinase in late versus early endosomes. *J. Cell Sci.* 119:1219–1232. https://doi.org/10.1242/jcs.02833

Kadouri, N., S. Nevo, Y. Goldfarb, and J. Abramson. 2020. Thymic epithelial cell heterogeneity: TEC by TEC. *Nat. Rev. Immunol.* 20:239–253. https://doi.org/10.1038/s41577-019-0238-0

Kaushik, S., and A.M. Cuervo. 2018. The coming of age of chaperone-mediated autophagy. *Nat. Rev. Mol. Cell Biol.* 19:365–381. https://doi.org/10.1038/s41580-018-0001-6

Klein, L., B. Kyewski, P.M. Allen, and K.A. Hogquist. 2014. Positive and negative selection of the T cell repertoire: What thymocytes see (and don't see). *Nat. Rev. Immunol.* 14:377–391. https://doi.org/10.1038/nri3667

Kondo, K., K. Takada, and Y. Takahama. 2017. Antigen processing and presentation in the thymus: Implications for T cell repertoire selection. *Curr. Opin. Immunol.* 46:53–57. https://doi.org/10.1016/j.coi.2017.03.014

Lantz, O., I. Grandjean, P. Matzinger, and J.P. Di Santo. 2000. Gamma chain required for naive CD4$^+$ T cell survival but not for antigen proliferation. *Nat. Immunol.* 1:54–58. https://doi.org/10.1038/76917

Levine, B., and G. Kroemer. 2019. Biological functions of autophagy genes: A disease perspective. *Cell*. 176:11–42. https://doi.org/10.1016/j.cell.2018.09.048

Li, L., Z.V. Wang, J.A. Hill, and F. Lin. 2014. New autophagy reporter mice reveal dynamics of proximal tubular autophagy. *J. Am. Soc. Nephrol.* 25:305–315. https://doi.org/10.1681/ASN.2013040374

Lucas, B., A.J. White, E.J. Cosway, S.M. Parnell, K.D. James, N.D. Jones, I. Ohigashi, Y. Takahama, W.E. Jenkinson, and G. Anderson. 2020. Diversity in medullary thymic epithelial cells controls the activity and availability of iNKT cells. *Nat. Commun.* 11:2198. https://doi.org/10.1038/s41467-020-16041-x

Ma, T., J. Li, Y. Xu, C. Yu, T. Xu, H. Wang, K. Liu, N. Cao, B.M. Nie, S.Y. Zhu, et al. 2015. Atg5-independent autophagy regulates mitochondrial clearance and is essential for iPSC reprogramming. *Nat. Cell Biol.* 17:1379–1387. https://doi.org/10.1038/ncb3256

Madisen, L., T.A. Zwingman, S.M. Sunkin, S.W. Oh, H.A. Zariwala, H. Gu, L.L. Ng, R.D. Palmiter, M.J. Hawrylycz, A.R. Jones, et al. 2010. A robust and high-throughput Cre reporting and characterization system for the whole mouse brain. *Nat. Neurosci.* 13:133–140. https://doi.org/10.1038/nn.2467

Manley, N.R., E.R. Richie, C.C. Blackburn, B.G. Condie, and J. Sage. 2011. Structure and function of the thymic microenvironment. *Front. Biosci.* 16:2461–2477. https://doi.org/10.2741/3866

Martin, W.D., G.G. Hicks, S.K. Mendiratta, H.I. Leva, H.E. Ruley, and L. Van Kaer. 1996. H2-M mutant mice are defective in the peptide loading of class II molecules, antigen presentation, and T cell repertoire selection. *Cell*. 84:543–550. https://doi.org/10.1016/s0092-8674(00)81030-2

Martinez-Martin, N., P. Maldonado, F. Gasparrini, B. Frederico, S. Aggarwal, M. Gaya, C. Tsui, M. Burbage, S.J. Keppler, B. Montaner, et al. 2017. A switch from canonical to noncanonical autophagy shapes B cell responses. *Science*. 355:641–647. https://doi.org/10.1126/science.aal3908

Martinez-Ruiz, G.U., A. Morales-Sanchez, and A. Bhandoola. 2022. Transcriptional and epigenetic regulation in thymic epithelial cells. *Immunol. Rev.* 305:43–58. https://doi.org/10.1111/imr.13034

Martinez, J., L.D. Cunha, S. Park, M. Yang, Q. Lu, R. Orchard, Q.Z. Li, M. Yan, L. Janke, C. Guy, et al. 2016. Noncanonical autophagy inhibits the autoinflammatory, lupus-like response to dying cells. *Nature*. 533:115–119. https://doi.org/10.1038/nature17950

Martinez, J., R.K.S. Malireddi, Q. Lu, L.D. Cunha, S. Pelletier, S. Gingras, R. Orchard, J.L. Guan, H. Tan, J. Peng, et al. 2015. Molecular characterization of LC3-associated phagocytosis reveals distinct roles for Rubicon, NOX2 and autophagy proteins. *Nat. Cell Biol.* 17:893–906. https://doi.org/10.1038/ncb3192

Mayassi, T., L.B. Barreiro, J. Rossjohn, and B. Jabri. 2021. A multilayered immune system through the lens of unconventional T cells. *Nature*. 595:501–510. https://doi.org/10.1038/s41586-021-03578-0

Mendiratta, S.K., W.D. Martin, S. Hong, A. Boesteanu, S. Joyce, and L. Van Kaer. 1997. CD1d1 mutant mice are deficient in natural T cells that promptly produce IL-4. *Immunity*. 6:469–477. https://doi.org/10.1016/s1074-7613(00)80290-3

Milam, A.V., and P.M. Allen. 2015. Functional heterogeneity in CD4(+) T cell responses against a bacterial pathogen. *Front. Immunol.* 6:621. https://doi.org/10.3389/fimmu.2015.00621

Miller, S.D., W.J. Karpus, and T.S. Davidson. 2010. Experimental autoimmune encephalomyelitis in the mouse. *Curr. Protoc. Immunol.* Chapter 15:Unit 15.1. https://doi.org/10.1002/0471142735.im1501s88

Miqueu, P., M. Guillet, N. Degauque, J.C. Dore, J.P. Soulillou, and S. Brouard. 2007. Statistical analysis of CDR3 length distributions for the assessment of T and B cell repertoire biases. *Mol. Immunol.* 44:1057–1064. https://doi.org/10.1016/j.molimm.2006.06.026

Mizushima, N., A. Yamamoto, M. Matsui, T. Yoshimori, and Y. Ohsumi. 2004. In vivo analysis of autophagy in response to nutrient starvation using transgenic mice expressing a fluorescent autophagosome marker. *Mol. Biol. Cell*. 15:1101–1111. https://doi.org/10.1091/mbc.e03-09-0704

Munz, C. 2018. Non-canonical functions of macroautophagy proteins during endocytosis by myeloid antigen presenting cells. *Front. Immunol.* 9:2765. https://doi.org/10.3389/fimmu.2018.02765

Nakagawa, T., W. Roth, P. Wong, A. Nelson, A. Farr, J. Deussing, J.A. Villadangos, H. Ploegh, C. Peters, and A.Y. Rudensky. 1998. Cathepsin L: Critical role in Ii degradation and CD4 T cell selection in the thymus. *Science*. 280:450–453. https://doi.org/10.1126/science.280.5362.450

Nedjic, J., M. Aichinger, J. Emmerich, N. Mizushima, and L. Klein. 2008. Autophagy in thymic epithelium shapes the T-cell repertoire and is essential for tolerance. *Nature*. 455:396–400. https://doi.org/10.1038/nature07208

Nikolic-Zugic, J., and M.J. Bevan. 1990. Functional and phenotypic delineation of two subsets of CD4 single positive cells in the thymus. *Int. Immunol.* 2:135–141. https://doi.org/10.1093/intimm/2.2.135

Nishida, Y., S. Arakawa, K. Fujitani, H. Yamaguchi, T. Mizuta, T. Kanaseki, M. Komatsu, K. Otsu, Y. Tsujimoto, and S. Shimizu. 2009. Discovery of Atg5/Atg7-independent alternative macroautophagy. *Nature*. 461:654–658. https://doi.org/10.1038/nature08455

Pacholczyk, R., H. Ignatowicz, P. Kraj, and L. Ignatowicz. 2006. Origin and T cell receptor diversity of Foxp3$^+$CD4$^+$CD25$^+$ T cells. *Immunity*. 25:249–259. https://doi.org/10.1016/j.immuni.2006.05.016

Pannetier, C., M. Cochet, S. Darche, A. Casrouge, M. Zoller, and P. Kourilsky. 1993. The sizes of the CDR3 hypervariable regions of the murine T-cell receptor beta chains vary as a function of the recombined germ-line segments. *Proc. Natl. Acad. Sci. USA*. 90:4319–4323. https://doi.org/10.1073/pnas.90.9.4319

Parekh, V.V., S.K. Pabbisetty, L. Wu, E. Sebzda, J. Martinez, J. Zhang, and L. Van Kaer. 2017. Autophagy-related protein Vps34 controls the homeostasis and function of antigen cross-presenting CD8α$^+$ dendritic cells. *Proc. Natl. Acad. Sci. USA*. 114:E6371–E6380. https://doi.org/10.1073/pnas.1706504114

Parekh, V.V., L. Wu, K.L. Boyd, J.A. Williams, J.A. Gaddy, D. Olivares-Villagomez, T.L. Cover, W.X. Zong, J. Zhang, and L. Van Kaer. 2013. Impaired autophagy, defective T cell homeostasis, and a wasting syndrome in mice with a T cell-specific deletion of Vps34. *J. Immunol.* 190:5086–5101. https://doi.org/10.4049/jimmunol.1202071

Ramsdell, F., M. Jenkins, Q. Dinh, and B.J. Fowlkes. 1991. The majority of CD4$^+$8$^-$ thymocytes are functionally immature. *J. Immunol.* 147:1779–1785

Reifler, A., X. Li, A.J. Archambeau, J.R. McDade, N. Sabha, D.E. Michele, and J.J. Dowling. 2014. Conditional knockout of pik3c3 causes a murine muscular dystrophy. *Am. J. Pathol.* 184:1819–1830. https://doi.org/10.1016/j.ajpath.2014.02.012

Roche, P.A., and K. Furuta. 2015. The ins and outs of MHC class II-mediated antigen processing and presentation. *Nat. Rev. Immunol.* 15:203–216. https://doi.org/10.1038/nri3818

Rodrigues, P.M., L.G. Sousa, C. Perrod, A.R. Maceiras, P. Ferreirinha, R. Pombinho, G. Romera-Cardenas, M. Gomez-Lazaro, M. Senkara, J. Pistolic, et al. 2022. LAMP2 regulates autophagy in the thymic epithelium and thymic stroma-dependent CD4 T cell development. *Autophagy*:1–14. https://doi.org/10.1080/15548627.2022.2074105

Ronan, B., O. Flamand, L. Vescovi, C. Dureuil, L. Durand, F. Fassy, M.F. Bachelot, A. Lamberton, M. Mathieu, T. Bertrand, et al. 2014. A highly potent and selective Vps34 inhibitor alters vesicle trafficking and autophagy. *Nat. Chem. Biol.* 10:1013–1019. https://doi.org/10.1038/nchembio.1681

Row, P.E., B.J. Reaves, J. Domin, J.P. Luzio, and H.W. Davidson. 2001. Overexpression of a rat kinase-deficient phosphoinositide 3-kinase, Vps34p, inhibits cathepsin D maturation. *Biochem. J.* 353:655–661. https://doi.org/10.1042/0264-6021:3530655

Savage, P.A., D.E.J. Klawon, and C.H. Miller. 2020. Regulatory T cell development. *Annu. Rev. Immunol.* 38:421–453. https://doi.org/10.1146/annurev-immunol-100219-020937

Schmid, D., M. Pypaert, and C. Munz. 2007. Antigen-loading compartments for major histocompatibility complex class II molecules continuously receive input from autophagosomes. *Immunity*. 26:79–92. https://doi.org/10.1016/j.immuni.2006.10.018

Schuster, C., K.D. Gerold, K. Schober, L. Probst, K. Boerner, M.J. Kim, A. Ruckdeschel, T. Serwold, and S. Kissler. 2015. The autoimmunity-associated gene CLEC16A modulates thymic epithelial cell autophagy and alters T cell selection. *Immunity*. 42:942–952. https://doi.org/10.1016/j.immuni.2015.04.011

Smith, N.L., R.K. Patel, A. Reynaldi, J.K. Grenier, J. Wang, N.B. Watson, K. Nzingha, K.J. Yee Mon, S.A. Peng, A. Grimson, et al. 2018. Developmental origin governs CD8(+) T cell fate decisions during infection. *Cell*. 174:117–130.e14. https://doi.org/10.1016/j.cell.2018.05.029

Song, W., Y. Ma, J. Wang, D. Brantley-Sieders, and J. Chen. 2014. JNK signaling mediates EPHA2-dependent tumor cell proliferation, motility, and cancer stem cell-like properties in non-small cell lung cancer. *Cancer Res.* 74:2444–2454. https://doi.org/10.1158/0008-5472.CAN-13-2136

Sudhakar, J.N., H.H. Lu, H.Y. Chiang, C.S. Suen, M.J. Hwang, S.Y. Wu, C.N. Shen, Y.M. Chang, F.A. Li, F.T. Liu, and J.W. Shui. 2020. Lumenal Galectin-9-Lamp2 interaction regulates lysosome and autophagy to prevent pathogenesis in the intestine and pancreas. *Nat. Commun.* 11:4286. https://doi.org/10.1038/s41467-020-18102-7

Takaba, H., and H. Takayanagi. 2017. The mechanisms of T cell selection in the thymus. *Trends Immunol.* 38:805–816. https://doi.org/10.1016/j.it.2017.07.010

Van Kaer, L., V.V. Parekh, J.L. Postoak, and L. Wu. 2019. Role of autophagy in MHC class I-restricted antigen presentation. *Mol. Immunol.* 113:2–5. https://doi.org/10.1016/j.molimm.2017.10.021

Ventura, A., D.G. Kirsch, M.E. McLaughlin, D.A. Tuveson, J. Grimm, L. Lintault, J. Newman, E.E. Reczek, R. Weissleder, and T. Jacks. 2007. Restoration of p53 function leads to tumour regression in vivo. *Nature*. 445:661–665. https://doi.org/10.1038/nature05541

von Rohrscheidt, J., E. Petrozziello, J. Nedjic, C. Federle, L. Krzyzak, H.L. Ploegh, S. Ishido, A. Steinkasserer, and L. Klein. 2016. Thymic CD4 T cell selection requires attenuation of March8-mediated MHCII turnover in cortical epithelial cells through CD83. *J. Exp. Med.* 213:1685–1694. https://doi.org/10.1084/jem.20160316

Wertheimer, T., E. Velardi, J. Tsai, K. Cooper, S. Xiao, C.C. Kloss, K.J. Ottmuller, Z. Mokhtari, C. Brede, P. deRoos, et al. 2018. Production of BMP4 by endothelial cells is crucial for endogenous thymic regeneration. *Sci. Immunol.* 3:eaal2736. https://doi.org/10.1126/sciimmunol.aal2736

Wong, J., R. Obst, M. Correia-Neves, G. Losyev, D. Mathis, and C. Benoist. 2007. Adaptation of TCR repertoires to self-peptides in regulatory and nonregulatory CD4$^+$ T cells. *J. Immunol.* 178:7032–7041. https://doi.org/10.4049/jimmunol.178.11.7032

Wong, K., N.L. Lister, M. Barsanti, J.M.C. Lim, M.V. Hammett, D.M. Khong, C. Siatskas, D.H.D. Gray, R.L. Boyd, and A.P. Chidgey. 2014. Multilineage potential and self-renewal define an epithelial progenitor cell population in the adult thymus. *Cell Rep.* 8:1198–1209. https://doi.org/10.1016/j.celrep.2014.07.029

Yang, G., J.L. Postoak, W. Song, J. Martinez, J. Zhang, L. Wu, and L. Van Kaer. 2022. Dendritic cell PIK3C3/VPS34 controls the pathogenicity of CNS autoimmunity independently of LC3-associated phagocytosis. *Autophagy*. 18:161–170. https://doi.org/10.1080/15548627.2021.1922051

Zhou, X., L. Wang, H. Hasegawa, P. Amin, B.X. Han, S. Kaneko, Y. He, and F. Wang. 2010. Deletion of PIK3C3/Vps34 in sensory neurons causes rapid neurodegeneration by disrupting the endosomal but not the autophagic pathway. *Proc. Natl. Acad. Sci. USA*. 107:9424–9429. https://doi.org/10.1073/pnas.0914725107

Supplemental material

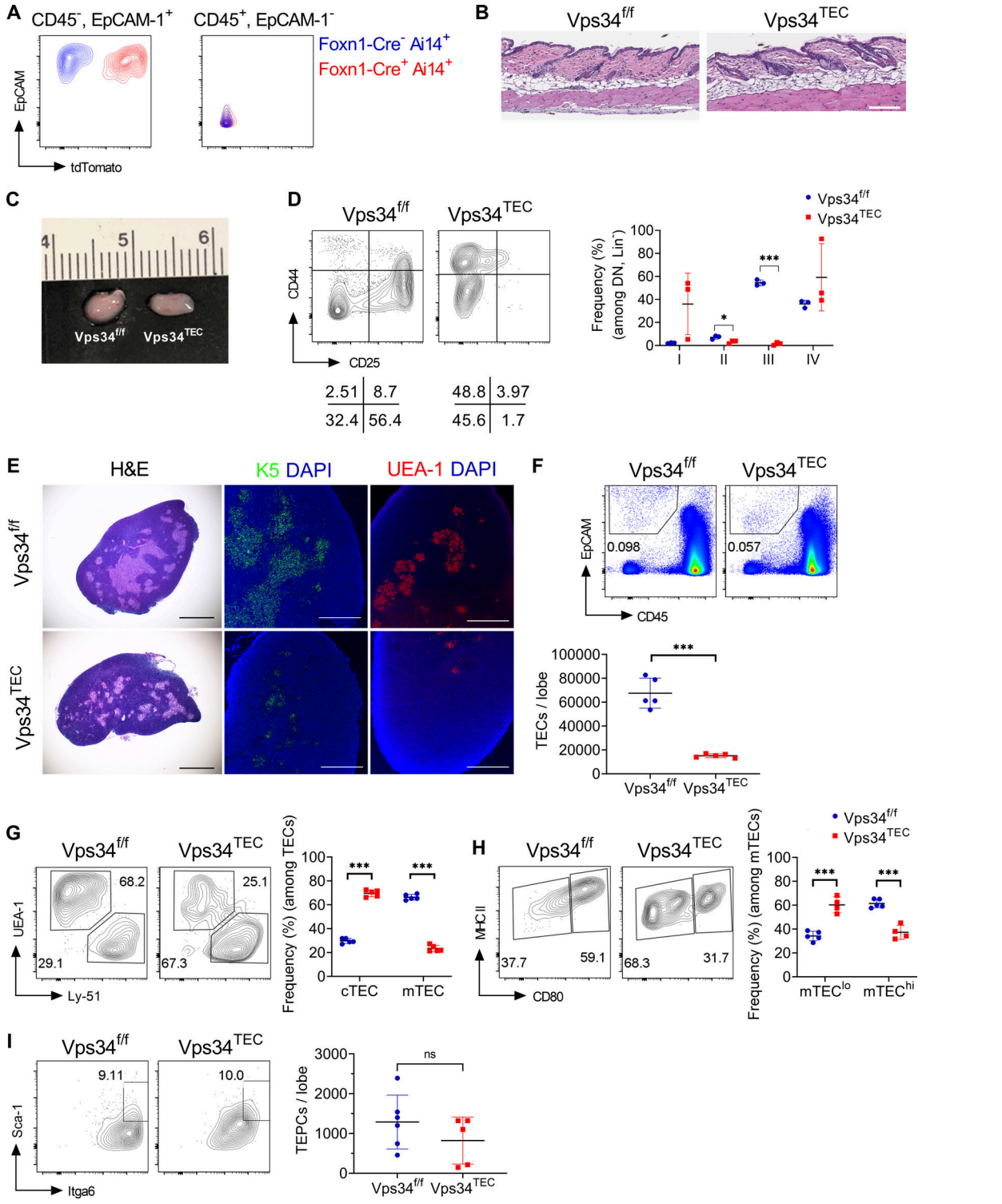

Figure S1. **Vps34^{TEC} phenotype. (A)** Flow cytometric analysis of TECs (CD45$^-$EpCAM$^+$) and thymocytes (CD45$^+$, EpCAM$^-$) for tdTomato expression isolated from 1-wk-old Foxn1-Cre$^-$Ai14$^+$ or Foxn1-Cre$^+$Ai14$^+$ mice. **(B)** Dorsal skin tissue sections from 8-wk-old Vps34$^{f/f}$ or Vps34^{TEC} mice stained with H&E (scale bar = 100 µm). **(C)** Gross images of thymic lobes isolated from 1-wk-old Vps34$^{f/f}$ or Vps34^{TEC} mice. **(D)** Flow cytometric analysis of CD4$^-$CD8$^-$Lin (CD3, B220, NK1.1)$^-$ DN thymocytes including DNI (CD44$^+$CD25$^-$), DNII (CD44$^+$CD25$^+$), DNIII (CD44$^-$CD25$^+$), and DNIV (CD44$^-$CD25$^-$) isolated from 6- to 8-wk-old Vps34$^{f/f}$ and Vps34^{TEC} mice. The graph represents the relative frequency of each indicated DN thymocyte population. **(E)** Thymus tissue sections from 7- to 10-d-old Vps34$^{f/f}$ or Vps34^{TEC} mice stained with H&E (scale bar = 1,000 µm), anti-keratin 5 (K5; green) and DAPI (blue), or UEA-1 lectin (red) and DAPI (blue; scale bar = 500 µm). **(F and G)** Flow cytometric analysis of (F) total TECs and (G) TEC subsets, including mTECs (UEA-1$^+$Ly-51$^-$) and cTECs (UEA-1$^-$Ly-51$^+$) at 10 d of age. **(H)** mTEC^{hi} (MHC II^{hi}CD80^{hi}) and mTEC^{lo} (MHC II^{lo}CD80^{lo}) frequency among mTECs. **(I)** Sca-1 and Itga-6 expression by UEA-1^{lo} TECs. The graph represents Sca-1$^+$Itga6$^+$ cells among UEA-1^{lo} TECs. Data are representative of at least two independent experiments with at least two mice per group. Each graphed data point represents a biological replicate. Data signify the mean ± SD. *, P < 0.05; ***, P < 0.001; ns, not significant by unpaired *t* test.

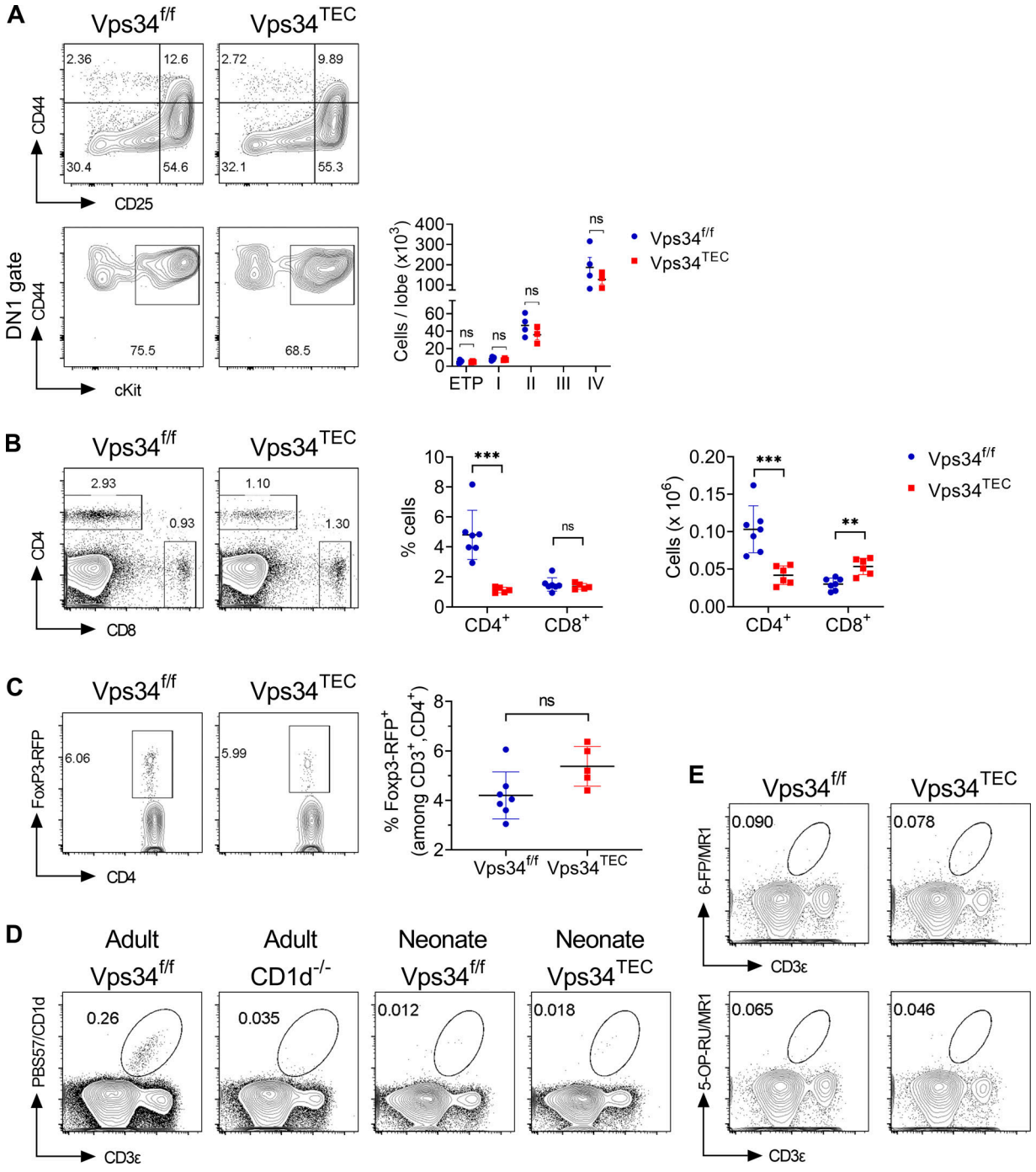

Figure S2. **DN thymocytes, iNKT cells, MAIT cells, and splenic T cells in neonatal Vps34^{TEC} mice. (A)** Flow cytometric analysis of CD4$^-$CD8$^-$Lin (CD3, B220, NK1.1)$^-$ DN thymocytes including DNI (CD44$^+$CD25$^-$), DNII (CD44$^+$CD25$^+$), DNIII (CD44$^-$CD25$^+$), DNIV (CD44$^-$CD25$^-$), and ETPs (CD44$^+$CD25$^-$cKit$^+$) isolated from 3-d-old Vps34$^{f/f}$ and Vps34^{TEC} mice. The graph represents total numbers of the indicated thymocyte subset per thymic lobe. Data obtained from two independent experiments (n = 3–4 biological replicates per genotype). **(B and C)** Splenocytes from 3-d-old Vps34$^{f/f}$ or Vps34^{TEC} mice were analyzed by flow cytometry. Flow cytometric analysis of (B) CD4 and CD8 expression, and (C) Foxp3-RFP expression among CD4$^+$ T cells (CD3$^+$CD4$^+$). Graphs represent frequency and total numbers of the indicated splenic subsets. Data obtained from three independent experiments (n = 5–7 mice per genotype). **(D)** Flow cytometric analysis of iNKT cells (PBS57/CD1d-tetramer$^+$CD3$^+$) isolated from the thymus of the indicated mouse strains at the indicated ages. **(E)** Flow cytometric analysis of MAIT cells (5-OP-RU/MR1-tetramer$^+$CD3$^+$) isolated from 3-d-old Vps34$^{f/f}$ or Vps34^{TEC} mice. As a control, cells were stained with 6-FP/MR1-tetramers (top). Data obtained from two independent experiments with at least three biological replicates. Data signify the mean ± SD where each graphed data point represents a biological replicate. **, P < 0.01; ***, P < 0.001; ns, not significant by unpaired t test.

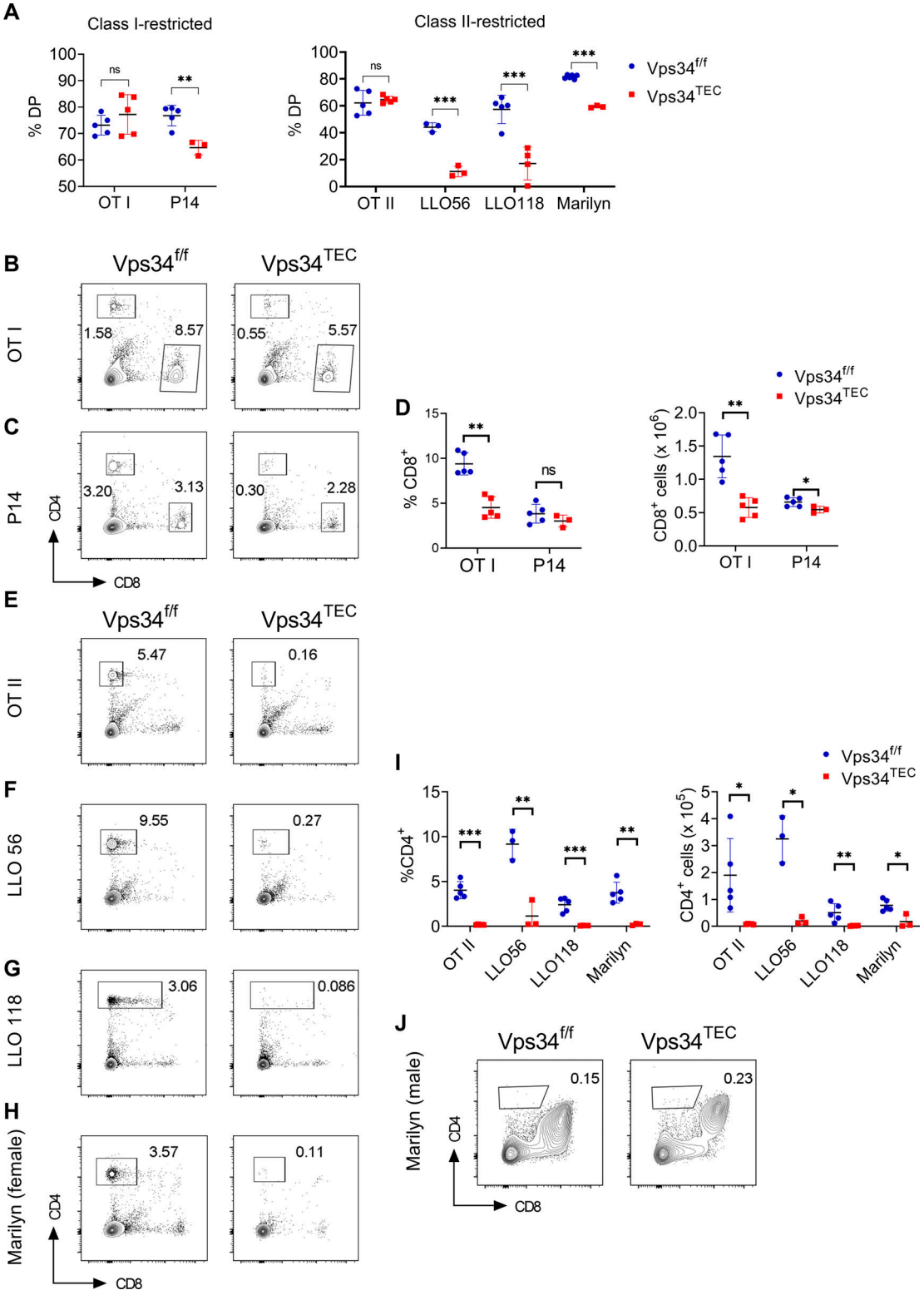

Figure S3. **Splenic phenotype of T cells in TCR transgenic mice. (A)** DP thymocyte frequency of 1-wk-old Vps34$^{f/f}$ or Vps34^{TEC} mice transgenic for the indicated MHC class I–restricted (left) or MHC class II–restricted (right) TCRs. **(B and C)** Flow cytometric analysis of splenocytes for CD4 and CD8 expression from the following MHC class I–restricted TCR transgenic lines: (B) OTI and (C) P14. **(D)** Frequency (left) and total cell number (right) of CD8 SP cells in the indicated TCR lines. **(E–H)** Flow cytometric analysis of splenocytes for CD4 and CD8 expression from the following MHC class II–restricted TCR transgenic lines: (E) OTII, (F) LLO56, (G) LLO118, and (H) Marilyn (females only). **(I)** Frequency (left) and total cell number (right) of CD4 SP in the indicated transgenic TCR lines. **(J)** Marilyn thymocyte development in male Vps34^{TEC} and Vps34$^{f/f}$ mice. Data signify the mean ± SD. Data are representative of at least two independent experiments (n = 3–6 mice per genotype) where each data point represents a biological replicate. *, P < 0.05; **, P < 0.01; ***, P < 0.001; ns, not significant by unpaired t test.

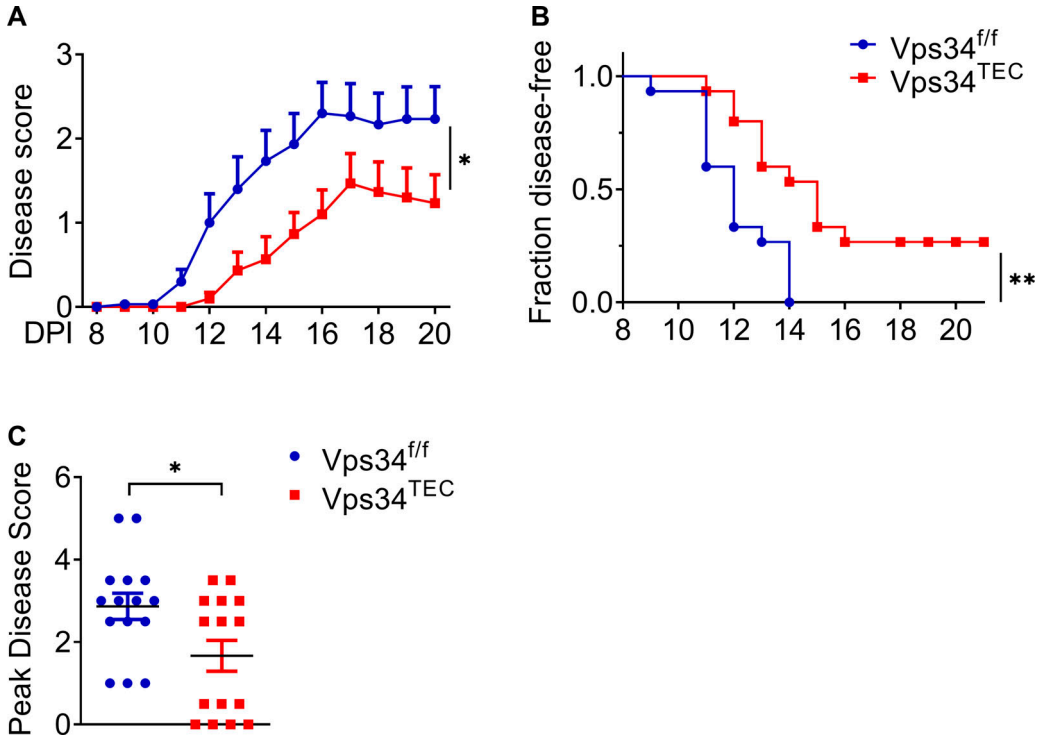

Figure S4. **Vps34 deficiency attenuates the incidence and severity of active EAE.** EAE was induced by active immunization with $MOG_{35–55}$ peptide. **(A)** Daily clinical score (ANOVA). **(B)** Disease onset (Kaplan–Meier curves by log-rank test). **(C)** Peak disease score (unpaired *t* test). Results are accumulated from three independent experiments with a combined total of 15 mice per group. The data shown are the average ± SEM. *, P < 0.05; **, P < 0.01; dpi, days postimmunization.

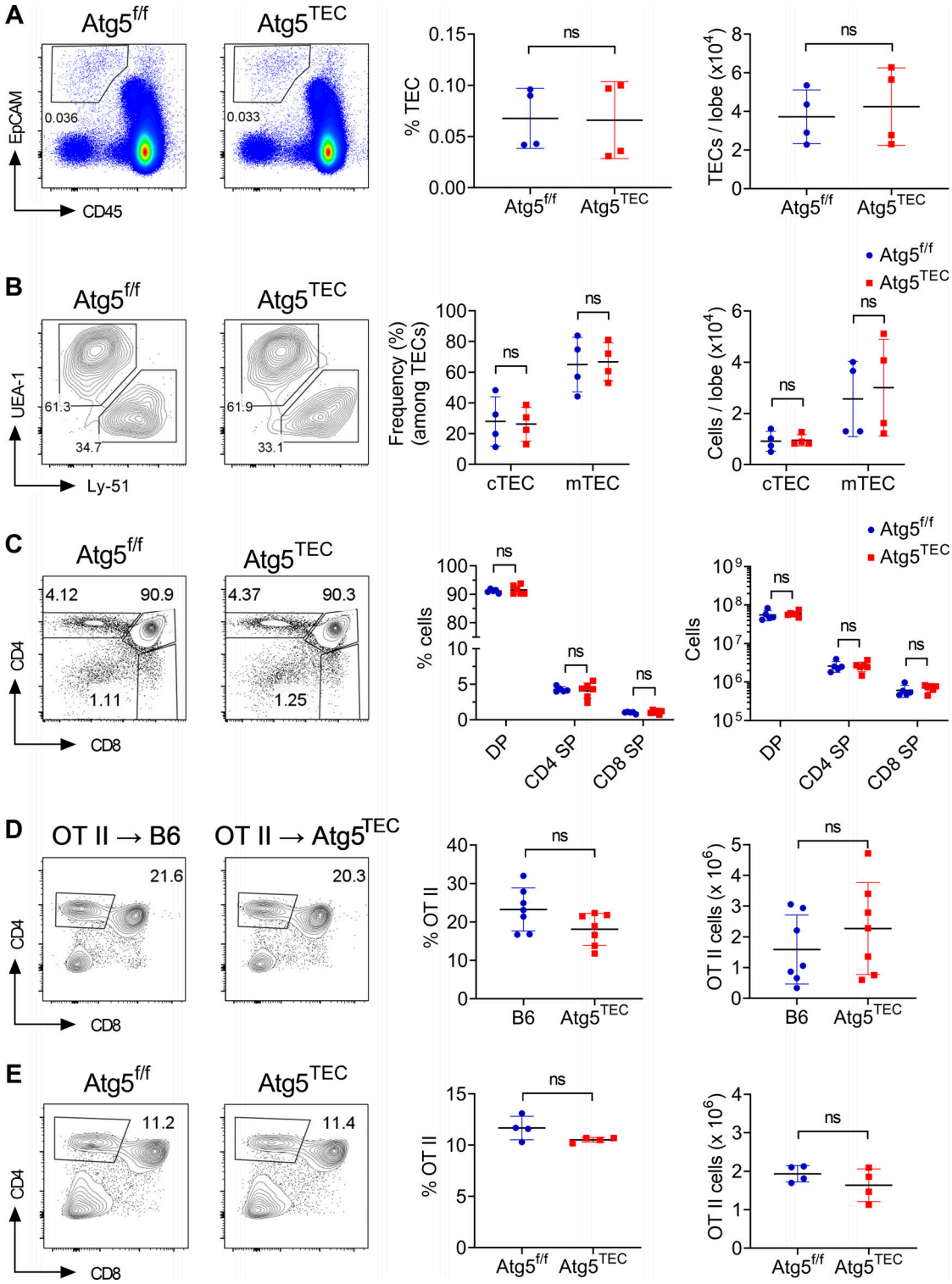

Figure S5. **Vps34 regulates CD4⁺ T cell positive selection in a canonical autophagy-independent mechanism. (A and B)** Flow cytometric analysis of (A) total TECs (CD45⁻EpCAM⁺) and (B) TEC subsets, including mTECs (UEA-1⁺Ly-51⁻) and cTECs (UEA-1⁻Ly-51⁺) on postnatal day 10. Graphs represent frequency (left) and total number (right) of TECs or TEC subsets. Data obtained from two independent experiments (n = 4 mice per genotype). **(C–E)** Thymocytes were analyzed for CD4 and CD8 expression by flow cytometry. **(C)** Analysis of 10-d-old Atg5$^{f/f}$ or Atg5^{TEC} mice. Graphs represent frequency and total numbers of the indicated thymocyte subsets. Data obtained from two independent experiments (n = 5–6 mice per genotype). **(D)** B6 or Atg5^{TEC} mice 5 wk after lethal irradiation following engraftment with OTII TCR transgenic bone marrow. Graphs represent frequency and total numbers of OTII cells (CD4 SP TCR Vα2^{hi}). Data obtained from two independent experiments (n = 7 mice per group). **(E)** OTII TCR transgene was introgressed into the Atg5^{TEC} strain and offspring were analyzed for positive selection compared with OTII TCR transgenic Atg5$^{f/f}$ controls. Data obtained from two independent experiments (n = 4 mice per genotype). Graphs represent frequency and total numbers of OTII cells (CD4 SP TCR Vα2^{hi}). Data signify the mean ± SD where each data point represents a biological replicate. ns, not significant by unpaired t test.

Provided online are Table S1 and Table S2. Table S1 shows specificity of TCR transgenic mice used in this study. Table S2 lists mouse strains used in this study.